2012

Electroencephalography (EEG)-based brain computer interfaces for rehabilitation

Dandan Huang
Virginia Commonwealth University

School of Engineering
Virginia Commonwealth University

This is to certify that the dissertation prepared by Dandan Huang entitled "Electroencephalography (EEG)-based brain computer interfaces for rehabilitation" has been approved by her committee as satisfactory completion of the dissertation requirement for the degree of Doctoral of Philosophy.

Ou Bai, Ph.D., Director of Dissertation, School of Engineering

Ding-Yu Fei, Ph.D., School of Engineering

Azhar Rafiq, M.D., School of Medicine

Martin L. Lenhardt, Ph.D., School of Engineering

Kayvan Najarian, Ph.D., School of Engineering

Gerald Miller, Ph.D., Chair, Department of Biomedical Engineering, School of Engineering

Rosalyn Hobson, Ph.D., Associate Dean of Graduate Studies, School of Engineering

Charles J. Jennett, Ph.D., Dean, School of Engineering

F. Douglas Boudinot, Ph.D., Dean of the Graduate School

_____

Date

ELECTROENCEPHALOGRAPHY-BASED BRAIN-COMPUTER INTERFACES FOR REHABILITATION

A dissertation submitted in partial fulfillment of the requirements for the degree of Doctor of Philosophy at Virginia Commonwealth University.

By

DANDAN HUANG

M.S., Virginia Commonwealth University, 2009

B.S., Tianjin University, People's Republic of China, 2007

Director: Ou Bai, PH.D.

Assistant Professor, Department of Biomedical Engineering

Virginia Commonwealth University

Richmond, Virginia

May, 2012

Acknowledgments

I would like to express my gratitude to all the people who have given their heart whelming full support in making this project a magnificent experience. My foremost thank goes to my Ph.D. adviser Dr. Ou Bai. Without him, this dissertation would not have been successful. I thank him for his patience and support that carried me on through difficulties, and for his knowledge, insights and creativity that inspired me to explore and challenge the unknown.

I am very grateful to Dr. Ding-Yu Fei, who encouraged and supported me throughout these years when I'm in VCU. I always enjoy so much from the discussion with him about research and life. I also would like to thank Ms. Cai-Ting Fu, my colleagues at the EEG&BCI Lab, and my collaborators at Huazhong University of Science and Technology for their great help, and I really enjoyed the time we spent together.

I would like to acknowledge and thank the members of my dissertation committee, Dr. Azhar Rafiq, Dr. Martin L. Lenhardt and Dr. Kavyan Najarian for kindly consenting to serve on my graduate committee and for reviewing and advising on this dissertation.

Special thanks are given to my parents for their unconditional love, support and encouragement throughout my studies.

To my mom Hongwen and my dad Yun

Table of Contents

List of Abbreviations

ALS	Amyotrophic lateral sclerosis
ADL	Activities of daily living
AVONA	One-way analysis of variance
BCI	Brain-computer Interface
Bpm	Bits per minute
CNS	Central nervous system
CCA	Canonical correlation analysis
ERD	Event-related desynchronization
ERS	Event-related synchronization
EEG	Electroencephalography
ECoG	Electrocorticography
EMG	Electromyography

EOG	Electrooculography
ERP	Event-related potential
FP	False positive
FPR	False positive rate
FNR	False negative rate and true negative
fMRI	Functional magnetic resonance imaging
fNIR	Functional near-infrared imaging
GA	Genetic algorithmeature
GA-MLD	GA-based Mahalanobis Linear Distance Classifier
GS	Go/Stop
ITR	Information transfer rate
IC	Intentional control
ID	Idle
LT	Left turn

LFP	Local field potentials
MEG	Magnetoencephalography
MLD	Mahalanobis linear distance
MLP	Multilayer perceptron
NC	Non-control
OVA	One-vs-all classifier
PCA	Principle component analysis
PSD	Power spectrum density
PMA	Pre-motor area
PLS	Primary lateral sclerosis
PET	Positron emission tomography
RBF	Radial basis function
RT	Right turn
SMA	Supplementary motor area

SMR	Sensorimotor rhythm
SCP	Slow-cortical potential
SVM	Support vector machine
SLD	Surface Laplacian derivation
SSVEP	Steady state visual evoked potential
TP	True positive
TN	True negative
TPR	True positive rate

List of Figures

Page

List of Tables

Page

Abstract

Objective: Brain-computer interface (BCI) technologies have been the subject of study for the past decades to help restore functions for people with severe motor disabilities and to improve their quality of life. BCI research can be generally categorized by control signals (invasive/non-invasive) or applications (e.g. neuroprosthetics/brain-actuated wheelchairs), and efforts have been devoted to better understand the characteristics and possible uses of brain signals. The purpose of this research is to explore the feasibility of a non-invasive BCI system with the combination of unique sensorimotor-rhythm (SMR) features. Specifically, a 2D virtual wheelchair control BCI is implemented to extend the application of previously designed 2D cursor control BCI, and the feasibility of the prototype is tested in electroencephalography (EEG) experiments; guidance on enhancing system performance is provided by a simulation incorporating intelligent control approaches under different EEG decoding accuracies; pattern recognition methods are explored to provide optimized classification results; and a hybrid BCI system is built to enhance the usability of the wheelchair BCI system.

Methods: In the virtual wheelchair control study, a creative and user friendly control strategy was proposed, and a paradigm was designed in Matlab, providing a virtual environment for control experiments; five subjects performed physical/imagined left/right hand movements or non-control tasks to control the virtual wheelchair to move forward,

turn left/right or stop; 2-step classification methods were employed and the performance was evaluated by hit rate and control time. Feature analysis and time-frequency analysis were conducted to examine the spatial, temporal and frequency properties of the utilized SMR features, i.e. event-related desynchronization (ERD) and post-movement event-related synchronization (ERS). The simulation incorporated intelligent control methods, and evaluated navigation and positioning performance with/without obstacles under different EEG decoding accuracies, to better guide optimization. Classification methods were explored considering different feature sets, tuned classifier parameters and the simulation results, and a recommendation was provided to the proposed system. In the steady state visual evoked potential (SSVEP) system for hybrid BCI study, a paradigm was designed, and an electric circuit system was built to provide visual stimulus, involving SSVEP as another type of signal being used to drive the EEG BCI system. Experiments were conducted and classification methods were explored to evaluate the system performance.

Results: ERD was observed on both hemispheres during hand's movement or motor imagery; ERS was observed on the contralateral hemisphere after movement or motor imagery stopped; five subjects participated in the continuous 2D virtual wheelchair control study and 4 of them hit the target with 100% hit rate in their best set with motor imagery. The simulation results indicated that the average hit rate with 10 obstacles can get above 95% for pass-door tests and above 70% for positioning tests, with EEG decoding accuracies of 70% for Non-Idle signals and 80% for idle signals. Classification methods showed that with properly tuned parameters, an average of about 70%-80% decoding

accuracy for all the classifiers could be reached, which reached the requirements set by the simulation test. Initial test on the SSVEP BCI system exhibited high classification accuracy, which may extend the usability of the wheelchair system to a larger population when finally combined with ERD/ERS BCI system.

Conclusion: This research investigated the feasibility of using both ERD and ERS associated with natural hand's motor imagery, aiming to implement practical BCI systems for the end users in the rehabilitation stage. The simulation with intelligent controls provided guides and requirements for EEG decoding accuracies, based on which pattern recognition methods were explored; properly selected features and adjusted parameters enabled the classifiers to exhibit optimal performance, suitable for the proposed system. Finally, to enlarge the population for which the wheelchair BCI system could benefit for, a SSVEP system for hybrid BCI was designed and tested. These systems provide a non-invasive, practical approach for BCI users in controlling assistive devices such as a virtual wheelchair, in terms of ease of use, adequate speed, and sufficient control accuracy.

CHAPTER 1

Introduction & Literature review

1.1 Background

Mobility limitations are the leading cause of functional limitations among adults with an estimated prevalence of 40 per 1000 persons aged 18 to 44 and 188 per 1000 aged 85 years and older in the general population [1]. Mobility difficulties are also strong predictors of difficulties with activities of daily living (ADL) and instrumental ADL, because individuals need to move to accomplish many of these activities. In addition, impaired mobility often decreases the opportunity to socialize, which results in social isolation, anxiety, and depression [2].

Amyotrophic lateral sclerosis (ALS) is a progressive neurodegenerative disease that affects nerve cells which are responsible for controlling voluntary movement. The first signs are muscle weakness and atrophy. Then, usually after 3-5 years, all voluntary movement is lost: the abilities to walk, speak, swallow, and breathe are all taken away. Because the disease does not affect sensations, intellect, or cognitive function, patients are left to watch their body slowly waste away. Muscle weakness and paralysis are characteristics of motor unit damage. Indeed, the pathology associated with ALS is the degeneration of the large alpha motor neurons. The large neurons of the motor cortex that innervate alpha motor neurons are also affected, but other neurons in the central nervous system (CNS) are spared. The

selective damage to motor neurons explains the selective loss of motor functions in ALS patients. Primary lateral sclerosis (PLS) is a variant of ALS that affects the corticospinal upper motor neurons, limiting movement. As some patients may completely lose motor function and become totally 'locked-in' [3], loss of motor function significantly affects patients' quality of life (QoL) [4-7] and increases the financial burden for the cost of care [8].

Unfortunately, motor recovery is not possible at present for patients with progressive diseases, such as ALS, PLS, multiple sclerosis, or Parkinson's disease, or for many patients with severe trauma due to stroke, cerebral palsy, or injury to the spinal cord or brain. Although some innovative rehabilitation strategies have shown potential in randomized controlled trials [9-12], available rehabilitation methods do not restore normal or near normal motor function and quality of life in most patients. Therefore, it is important to develop more effective alternative methods for people with motor disabilities.

1.2 Brain-computer interface technology

How is the movement generated? Let's take the arm movement of a healthy person for example. First, during the planning stage of movement, neurons in supplementary motor area (SMA) and premotor area (PMA) start firing, until the movement starts, and the primary motor cortex get activated mainly during the movement execution or even imagination; it will elicit twitches of muscles in the arm on the contralateral side.

For voluntary movement, the lateral pathways are involved where the brain talks to the spinal cord. The axons in the corticospinal tract originate in SMA, PMA and primary motor cortex and terminate in the ventral horns where the motor neurons control distal muscles. Alpha motor neurons directly generate force by activating extrafusal fibers in the muscle; meanwhile, gamma motor neurons stretch spindles by activating intrafusal fibers, and then send feedback to the spinal cord through Ia afferent. These events form a loop to complete muscle contraction.

For the patients whose neural pathways are blocked, a brain–computer interface (BCI) or brain–machine interface (BMI) has been proposed as an alternative communication pathway, bypassing the normal cortical-muscular pathway [13, 14]. BCI is a system that enhances neuromuscular output or provides a neural interface to substitute for the loss of normal neuromuscular outputs by enabling individuals to interact with their environment through brain signals rather than muscles [15, 16]. The signals that deliver user's communication or control intention are translated into an output, for example, cursor movement. The feedback on this output is received by the user through visual, auditory or tactile format; it in turn affects the user's brain activity and influences subsequent output. Recently there has been a great surge in research and development of brain-controlled devices for rehabilitation owing to increased societal interest and appreciation of the serious needs and impressive potential of patients with severe motor disabilities [16, 17].

1.3 Brain signal detection methods

Brain signals can be detected and measured in many ways, such as methods of recording electrical activities, magnetic activities or magnetoencephalography (MEG), functional magnetic resonance imaging (fMRI), functional near-infrared imaging (fNIR), and positron emission tomography (PET). However, due to the complex technical requirements, expense and real-time capabilities, MEG, fMRI and PET are not suitable for everyday use at their current stage. Only electrical field recording and fNIR [18] are likely to have practical value for clinical use in the near future.

Electrical activities of the brain can be recorded at the scalp (EEG), at the cortical surface (Electrocorticography or ECoG), or within the brain (local field potentials/LFP or spike train). Each method has its own advantages and disadvantages. ECoG and LFP methods have good topographical resolution and wide frequency ranges. The BCIs using invasive signal methods to record intracortical neuronal activities have shown great promise in direct brain control of external devices in primates, for example, to restore self-feeding by controlling a 3-D robotic arm [19]. However, they are invasive, requiring implantation of electrodes on the cortical surface or in the brain. The main concerns of invasive BCIs to be dealt with before clinical use include the following: long-term safety; the stability and duration of the signal; tissue reaction to the electrodes and whether it can outperform an alternative option such as a neuroprosthetic arm. Non-invasive EEG method has been

extensively explored because of its lower clinical threshold as well as the ease of use. But EEG recording is sometimes susceptible of being contaminated with electromyographic (EMG) or electrooculographic (EOG) activities from cranial muscles.

1.4 Challenges of EEG-based BCIs

In contrast to invasive methods, non-invasive methods feature an extremely low signal-to-noise (s/n) ratio, which is a major challenge in EEG based BCI development. Conventionally, s/n ratio can be improved by repeated averaging, for example, as in event-related potentials (ERPs), which can be obtained by averaging across trials time-locked to the stimuli. However, due to the requirement for repeated measurements, the communication speed is greatly reduced. An alternative method to improve s/n ratio for reliable BCI control is to train users to regulate their brain activity, such as by modulation of the slow-cortical potentials (SCP) [20] or the 8–12 Hz sensorimotor Mu rhythm [21]. Once people learn to effectively regulate their brain activity, reduction of the variance in the EEG signal can be expected and as a result, the s/n ratio is increased. However, due to the variance of spontaneous activity in EEG, long-term training is usually required for users to achieve effective and accurate regulation of either SCPs or sensorimotor Mu rhythms. The long-term training may require a couple of months to 1 or 2 years [22, 23]. Moreover, users may be easily fatigued from the sustained attention that is required to regulate their brain activities and as a result, render the BCI control unreliable.

Fatigue becomes serious in severely paralyzed patients who demonstrate not only reduced physical but also mental endurance [24, 25]. Recent pilot studies of BCI feasibility for ALS patients shows that they may not be able to learn the skills for effective regulation of brain activities because they are too weak to tolerate long-term training and/or active regulation with focused attention [26-28]. Although healthy persons or less severely paralyzed patients may operate current EEG based BCIs efficiently [29, 30], the performance of current BCIs in severely paralyzed patients with degenerative diseases such as ALS, however, was much lower because they were easily fatigued or could not tolerate long-term training. The accuracy was just over the random level for ALS patients, in contrast to the 90% accuracy level achieved in healthy subjects [23, 31]. Therefore, the inconvenience in operation may prevent current BCIs from practical clinical applications for severely paralyzed patients who are the users most in need of direct brain control of external devices to restore function.

1.5 Relevant studies by other groups

So far, systems based on EEG have been used to control a mouse on the screen [32], for communication like a speller [33, 34], an internet browser [35], or control a wheelchair [36-38]. The most commonly used feature in cursor or wheelchair control is event-related desynchronization (ERD) [39], a phenomenon of EEG amplitude attenuation during mental tasks indicating cortical activation. Through motor imagery of hand/foot movements by detecting spatially different ERD patterns, or through regulating brain rhythms to decrease

signal variability and increase SNR in order to discriminate control state ERD from non-control state baseline activity, users could achieve 1D, 2D cursor or wheelchair control [22, 38, 40-44]. Recently, 3D virtual helicopter control game [45] using intelligent control strategies [38, 44, 46-48] was reported, and 3D cursor control through right/left hand and foot motor imagery after a series of training sessions [49] has also been achieved. However, such kinds of methods usually require intensive user training. Approaches detecting only ERDs with left/right hand motor execution/imagery may experience insufficient decoding accuracy as there is evidence that during unilateral hand movement, ERD starts contralateral to the side of movement about 2s before movement onset and becomes bilateral at the time of movement onset [50-52]. Given that low detection error is more desirable in wheelchair control compared to applications in cursor control or computer games where speed is of higher importance and error tolerance is high, two questions arise: Is it possible to utilize new EEG features that may essentially provide higher separability among different mental tasks? Can we design a simple but effective paradigm to enhance the control accuracy and contribute in a fast attained 2D BCI for potential wheelchair control?

1.6 Preliminary studies by our group

In the preliminary studies of our group, we have identified that the human volition to move or cease to move associated with natural motor behavior can be reliably decoded online from EEG signals, where users do not need to learn vast training to regulate brain activities.

We found that the discrimination of ERD from ERS was much more reliable than the discrimination of ERD from background activities in conventional BCI methods [53, 54]. A short-lasting burst of EEG oscillation, termed as beta rebound or beta-ERS, has been observed in beta band (16–30 Hz) over human sensorimotor area after subjects produce a self-paced movement [39, 55, 56]. Although the beta rebound has been postulated as the result of afferent input [57], other studies show that the beta rebound does not necessarily depend on motor cortex output and muscle activation, and it may reflect a short-lasting state of deactivation or inhibition of the motor cortex [58, 59]. The feasibility of the beta rebound for BCI application derives from the fact that beta rebound may not only occur with real physical movement but also presents with motor imagery [60]. This comes into consideration since the patients who lose their voluntary muscle contraction may only imagine movement instead of producing real movement [53]. The beta rebound results in a strong synchronization, i.e. higher amplitude of rhythmic activities in beta band than background activities. As ERD features lower amplitude beta band activities, the discrimination of beta rebound or beta-ERS from beta-ERD is presumably more accurate than the discrimination of ERD from background activity. Furthermore, the beta rebound also features strict somatotopic organization [55], allowing for potential discrimination of different limb movements spatially according to human somatotopy. In 2008, our group implemented a synchronous sequential binary controls approach to decode EEGs to provide 2D control of a cursor on a computer screen, with simple threshold-based binary classification of band power readings taken over pre-defined time windows during subject right hand movement/motor imagery [53]. The following study, using spatial feature of the

beta rebound, supports a multi-dimensional BCI by reliable decoding of intentions to move individual limbs [61]. The beta-ERD and beta-ERS features associated with human natural motor control has also been further tested on six ALS or PLS patients in sequential binary control for 2D cursor control, and two patients further participated in direct two-dimensional cursor control in a single visit [62].

1.7 Aims of the doctoral study

In this doctoral study, further steps have been taken to explore the possibility of utilizing the ERD/ERS neurophysiological features to develop more advanced BCI systems that can better serve the potential users from multiple perspectives. The specific aims of this doctoral research are:

1. Design the prototype of a 2D virtual wheelchair control system and evaluate its feasibility. To develop an effective and practical 2D wheelchair control strategy based on the improved 2D cursor control rationale; design a paradigm of virtual environment; conduct wheelchair control experiments on healthy subjects; and perform feature analysis and statistical analysis to evaluate the system performance.

2. Explore classification methods and enhance the EEG decoding accuracy. A simulation will be done to set requirements for the decoding system. To achieve optimal classification performance, different parameters will be selected and tested

to optimize classification results, and recommendations will be made for the system according to the comparison result.

3. Enhance the usability of the wheelchair system with the final goal of achieving a hybrid BCI system. A SSVEP electric circuit system will be designed and built, to provide visual stimulus with flashing LEDs of different stimulation frequencies. The SSVEP system will be combined with ERS/ERS system in the future. The SSVEP system will be tested with subjects in EEG experiments.

To achieve the above research purposes, the hypotheses provided in this research are as follows:

1. The control rationale for 2D cursor movement can be transplanted and further improved into implementing a prototype of continuous wheelchair control, which subjects can quickly learn to operate with decent control accuracy and speed.

2. With intelligent control incorporated into the BCI system, requirements of EEG decoding accuracy could be looser and properly selected classifiers can easily satisfy the requirements.

3. The hybrid BCI by including visual stimulus can provide additional information that is useful for assisting classification. The performance of the SSVEP BCI is

expected to be comparable or superior with that of ERD/ERS BCI system, and the usability of the final hybrid system among the population should be enhanced.

CHAPTER 2

2D virtual wheelchair control

2.1 Experimental system

2.1.1 System hardware, software and electrodes set up

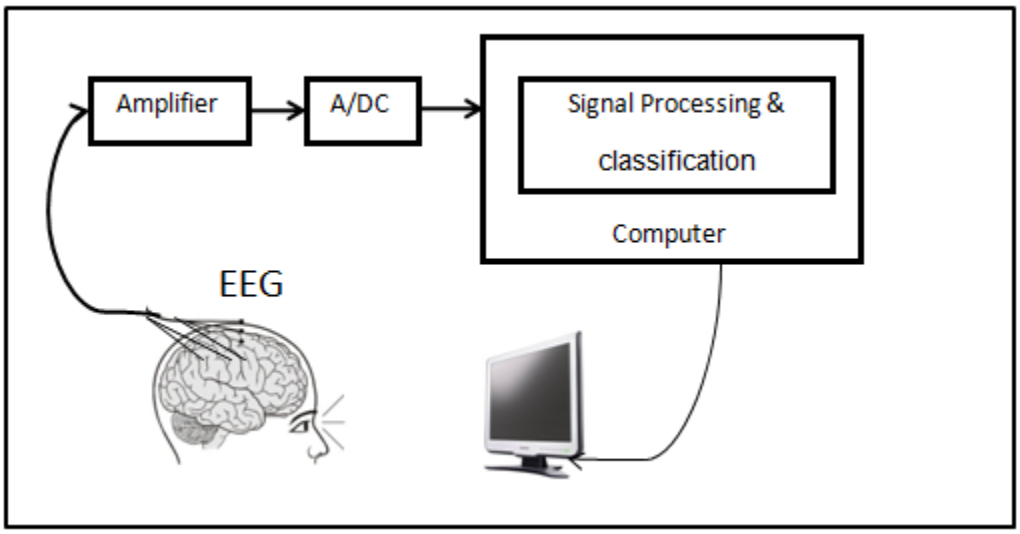

Figure 1. Experimental system. EEG signals were picked up from scalp and amplified, then were digitized through A/D convertor and sent to the computer for signal processing.

Figure 1 shows the system setup. A monitor was placed in front of the subject, presenting the experimental paradigm. Meanwhile, EEG signal was recorded from 27 (tin) surface electrodes attached on an elastic cap. Surface electromyography (EMG), which was used to monitor the movement and bipolar electrooculogram (EOG) above left eye and below right

eye were also recorded. The analog signals were amplified, and then digitized through A/D convertor. The digital signal was then sent to a computer for online processing.

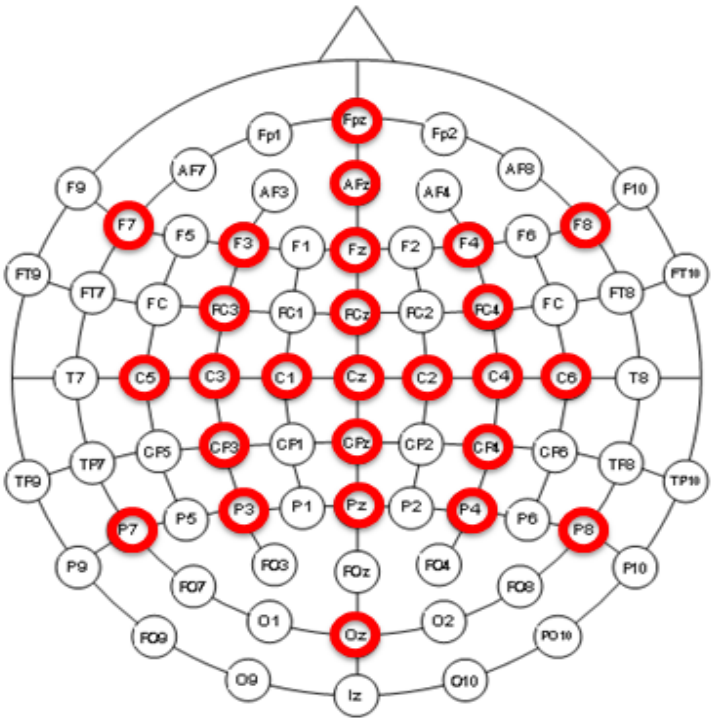

Figure 2. Electrodes setup.

EEG was recorded from 27 (tin) surface electrodes (Figure 2. F3, F7, C3A, C1, C3, C5, T3, C3P, P3, T5, F4, F8, C4A, C2, C4, C6, T4, C4P, P4, T6, FPZ, FZ, FCZ, CZ, CZP, PZ and OZ) attached on an elastic cap (Electro-Cap International, Inc., Eaton, OH, U.S.A.) according to the international 10-20 system [63], with reference from the right ear lobe and ground from the forehead. Two surface EMG electrodes were taped over the right and left wrist extensors, used to monitor the hand movement. Electrodes for bipolar EOG above left eye and below right eye were also pasted. Total duration of preparation for obtaining

consent, explaining paradigm, and setting up electrodes took around 30 min to 1 hour. Signals from all the channels were amplified (g.tec GmgH, Schiedlberg, Austria), filtered (0.1-100 Hz) and digitized (sampling frequency was 256 Hz). All impedances were kept below 5kΩ. The digital signal was processed online using a custom-made MATLAB (MathWorks, Natick, MA) Toolbox: brain-computer interface to virtual reality or BCI2VR [53, 64]. The paradigms were programmed in the BCI2VR, to provide the visual stimulus for the calibration, 2D virtual wheelchair control game, and online processing of the EEG signal.

2.2 Subject selection

2.2.1 General subject Inclusion criteria:

Subjects were selected based on normal neurologic and psychiatric history and examination, as well as a willingness and ability to perform simple voluntary movements over a 2-hour time period. Subjects were admitted to the protocol regardless of gender, race or ethnicity. Children were excluded as the movement parameters used in this study is less established in subjects under the age of 18. All subjects in this study were healthy volunteers.

2.2.2 Subject exclusion criteria:

We would exclude subjects who are unable to perform simple voluntary movement with both hands and subjects who have any neurological or psychiatric conditions. Ethnic origin

and race would not be a basis for inclusion or exclusion. We would strive to obtain a population sample that best represents the breakdown of this local area.

2.2.3 Potential risks

The risks of EEG and MEG are minimal. Subjects may feel uncomfortable while the electrodes are attached to their scalp, and they may not like the smell of the paste or the glue remover. The conductive gel sometimes causes some mild irritation. The substances used to remove the glue have quite a strong odor, but do not have any harmful effects when used for a short period of time. If human movement intention is predictable, future interventions can then be directed at using these EEG potentials to control prosthetic devices (brain-computer interfaces). This study would contribute to the understanding of how our brain prepares for movement and this may eventually lead to clinical applications; therefore, we believe that the benefits outweigh the minimal risk.

For the 2D virtual wheelchair control study, five right-handed healthy subjects (S1-S5, 2 females and 3 males) age 23 to 30 participated in. S2 had 6 hours BCI experience half a year ago for another irrelevant study; S1, S3-S5 had no previous BCI experience. All the subjects were participating for the first time in this study.

All the subjects gave informed consent before the studies, and both protocols were approved by the Institutional Review Board.

2.3 Experimental paradigm

2.3.1 Online wheelchair control paradigm

Figure 3 shows a set of small screen images (a-h) which demonstrate a sequence of steps in one target reaching task during the virtual wheelchair control. The converted real size of the simulated scenario is 20 by 20 square meters. The relative size of the targets on any of the four sides is 6 by 1 square meters. Each run began with the wheelchair at the center, and terminated when the wheelchair either hit the target (success) or at any time hit the edge elsewhere (failure). Subjects could inform the investigator to stop the experiment at any time; the investigator monitored the signal quality and EMG activity throughout the experimental procedure. The wheelchair moving speed was set to 0.4m/s, with a rotating speed of 27s per 360 degrees, within the common wheelchair speeds [65]. The wheelchair could move forward only in the direction of the blue bar, which always faced upwards at the beginning of each run. The wheelchair rotated with the square in its center as the axis. The square also served as the color cue; its color changes synchronized with the external auditory cues in different frequencies, reminding subjects of different task periods. Section 2.3.2 explains in detail how the wheelchair was controlled by performing mental tasks and shows the EEG patterns that were expected to be exhibited along with the tasks.

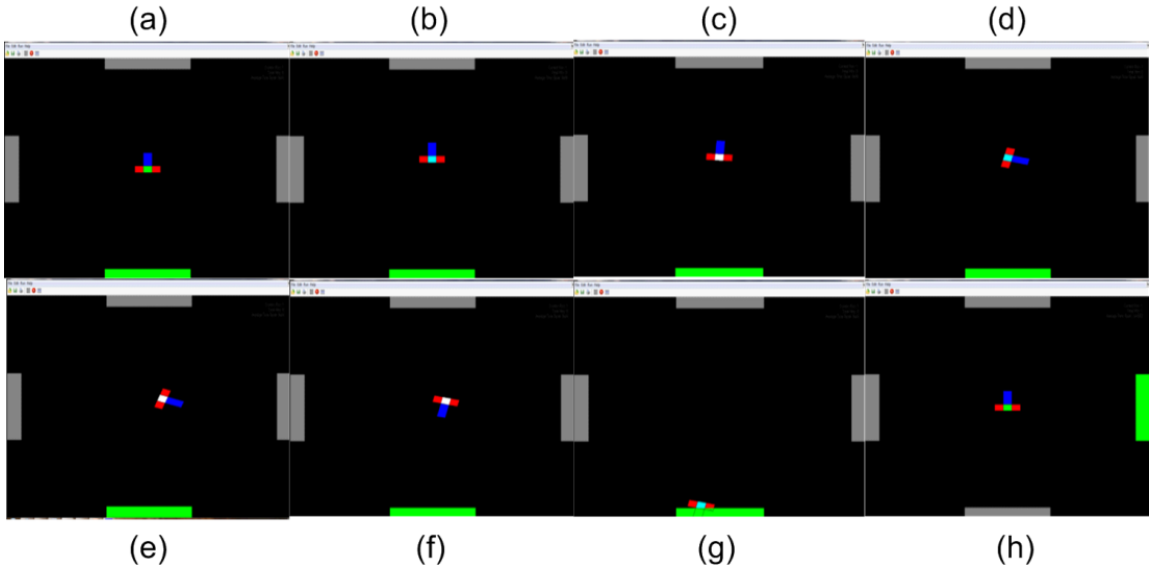

Figure 3. Screen shots of virtual wheelchair control in one run. (a) wheelchair started at the center of the screen-Stop State; (b) wheelchair started to move upward along the blue bar direction after receiving Go/Stop Command-Running State; (c) wheelchair started to make right turn after receiving Right Turn Command-Rotating State; (d) wheelchair stopped rotating and started to move along blue bar direction after receiving Go/Stop Command-Running State; (e) wheelchair stopped moving and started to make right turn after receiving Right Turn Command-Rotating State; (f) wheelchair stopped rotating and started to move along blue bar direction after receiving Go/Stop Command-Running State; (g) wheelchair reached the target-Stop State; (h) simulation of wheelchair control restarted-Stop State.

2.3.2 Wheelchair control strategy

Figure 4 shows the expected EEG power changes with execution of four mental tasks separately (in four rows). The performing of each task together with expected EEG power changes and output control command is visualized in Figure 4, and also summarized in Table 1. Take the top row for example. This is a "Go/Stop" command or "GS" for short. Task began with the T1 time window (0-1.5s), indicated by the color change of the color cue (the square in the center of the wheelchair changed to green) which occurred simultaneously with the first auditory cue onset. When this happened, subjects performed

right wrist extension or motor imagery (refer Table2). When the color cue changed to blue, T2 time window (1.5-4s) began and subject heard the second auditory beep as well. In this period, subjects continued performing right wrist extension or motor imagery until the end of T2 window, when the color cue changed to white and the third auditory cue onset. Movement intention was decoded and control action was taken: in this "GS" case, the virtual wheelchair started to move forward from the original stop state.

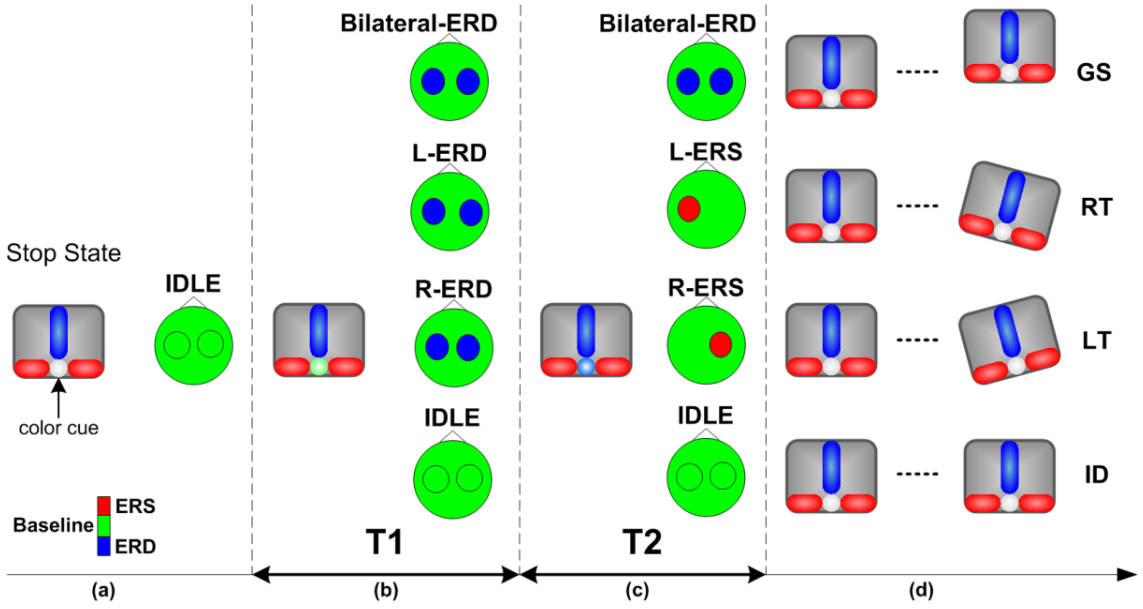

Figure 4. Strategy of wheelchair control. (a)-(d) follow the time sequence. (a) In stop state, the wheelchair is keeping still. (b) In the first cue period T1, subjects start any of the motor tasks; from top to bottom are the four situations: right wrist extension-left hemisphere ERD pattern, right wrist extension-left hemisphere ERD pattern, left wrist extension-right hemisphere ERD pattern or no motor task-Idle/baseline activity. (c) In the second cue period T2, subjects continue with the task: continue right wrist extension-left hemisphere ERD pattern, stop right wrist extension and relax-left hemisphere ERS, stop left wrist extension and relax-right hemisphere ERS, or no motor task-baseline activity. (d) Movement intention is decoded and wheelchair is driven to move forward (or stop when moving), turn right, turn left or keep current moving status. Inter-trial interval (the end of T2 to the beginning of next T1) is 2s.

Table 1. Wheelchair control commands, associated motor tasks, detected EEG patterns and output control actions

Control Command	Associated Motor Task		Detected Activity in T2	Control Actions	
	T1	T2		Current State	Next State
Go/Stop	Right wrist extension	Continued right wrist extension	Bilateral ERD	Stop	Running
				Running	Stop
				Rotating	Running
Right Turn	Right wrist extension	Relaxation	Left hemisphere ERS	Stop	Rotating
				Running	Rotating
Left Turn	Left wrist extension	Relaxation	Right hemisphere ERS	Stop	Rotating
				Running	Rotating
Idle State	No motor task	No motor task	Idle/resting activity	Any state	Unchanged

Specifically:

1. Go/Stop Command ('GS'): characterized by the bilateral ERD in both T1 and T2 windows, i.e. when users want the wheelchair to move forward, or stop the wheelchair when it is moving, they perform (imagined) right wrist extension continuously in both T1 and T2 windows. This command will make one of the following three possible state changes:

   I. Switch from Stop State to Running State, wheelchair will start moving;

   II. Switch from Running State to Stop State, wheelchair will stop moving;

   III. Switch from Rotating State to Running State, wheelchair will stop rotating and start to move.

2. Right Turn Command ('RT'): characterized by the bilateral ERD in T1 window and ERS on the left hemisphere in T2 window, i.e. when users want to make a right turn, they perform (imagined) right wrist extension in T1 window and stop the (imagined) movement at the beginning of T2 window. This command will make the following state change:

    I. Switch from Stop State or Running State to Rotating State, wheelchair will start to rotate to the right.

3. Left Turn Command ('LT'): characterized by the bilateral ERD in T1 window and ERS on the right hemisphere in T2 window, i.e. when users want to make a left turn, they perform (imagined) left wrist extension in T1 window and stop the (imagined) movement at the beginning of T2 window. This command will make the following state change:

    I. Switch from Stop State or Running State to Rotating State, wheelchair will start to rotate to the left.

The Idle ('ID')/non-control state is the natural state when subjects do not want to change moving state; whenever the computer detects 'ID' state, no control command will be sent out and thus the wheelchair keeps its current state. The involvement of 'ID' state in this study renders the continuous control and makes the control process easier.

2.4 Experiment procedure and Signal processing for decoding movement intention

For either physical or motor imagery session, each subject performed 25min of calibration, containing 96 'ID' tasks and 32 each of the other tasks ('GS', 'RT', 'LT'), with a 5min break in the middle. This created the models based on which subjects performed two sets of online wheelchair control games; each set had 8 runs/target reaching, two for each target location, with targets showing up pseudo-randomly. 1-5 minutes breaks were given in between games or runs.

2.4.1 Spatiotemporal filtering and feature selection

The online data were processed through three steps to decode the movement intention: (1) spatial filtering, (2) temporal filtering and (3) feature selection and classification.

The spatial filter applies a transformation matrix that is determined under certain constraints to the EEG signal so that the filtered signal may have a better signal-to-noise ratio for identifying the changes of the underlying neuronal sources. This procedure is similar to beam-forming, which can increase the gain in the direction of the task-related signals and decrease the gain in the direction of interference and noise. As a result, the spatial filter may improve classification accuracy. The signal from electrodes was directly fed into the temporal filter.

Surface Laplacian derivation (SLD) was applied as the spatial filter. SLD performs surface Laplacian transformation on multi-dimensional EEG signals. Realistic Laplacian transformation usually requires a head shape model, which can be constructed from brain imaging [66]. We employed a simple method, which is also called a 'reference-free' method so that the signal is independent of which electrode is used as reference. The EEG signal from each electrode was referenced to the averaged potentials from four orthogonal nearby electrodes [67]. SLD operation enhanced the spatial resolution of local EEG potentials by reducing the volume conduction effect. It applies a high-pass filter to suppress low-spatial frequency components along with volume conduction components so that the local synchronizations, in particular, their radial components, have increased spatial specificity [68] and as a result, the spatial difference following hand movements might be more discriminable.

Temporal filtering was done through the power spectral density (PSD) estimation of the spatially filtered EEG signal in the T1 and T2 window. According to the visual inspection of time–frequency plots of ERD and ERS after the calibration session, one period from T1 and one period from T2 were extracted in order to obtain the strongest ERD/ERS. PSD estimated power spectral densities of the spatial filtered signal using the Welch method. A Hamming window was employed to reduce side lobe effect. The FFT length was set to 0.256 s resulting in a frequency resolution of approximately 4 Hz. Power spectral densities were smoothed from segments with 50% overlapping. A number of PSD estimation

methods have been used in the signal processing literature, each of which varies in resolution and variance of the estimation. Periodogram or modified periodogram has higher spectral resolution, but the resulting variance is also larger than that of the Welch method [69]. The multitaper method provides a solution to balance the variance and resolution [70]. However, an optimal multitaper method permits the trade-off between resolution and variance to usually be data-dependent [71]. We did not employ parametric methods, for example, using autoregressive model coefficients [72]. The parametric model requires determining model order. Further, the model coefficients for classification are also indirect to frequencies, which are difficult for general neurophysiological analysis.

The spatially and temporally filtered EEG signals provided high-dimensional features; for example, 27 EEG channels with 16 frequency bins produced 432 features. Because of the noisy nature of EEG, such high-dimensional features may bias the classification model producing a low testing accuracy. A compact subset of features needs to be determined for achieving a robust classification. The subset feature selection can be determined either empirically or 'data-driven'. Because of the high dependence among features, the empirical approach usually does not provide a good solution. The exhaustive search method is one of the optimal feature selection methods, which evaluates all possible subsets to determine the best subsets. For example, the exhaustive search of a subset of 3 features from 432 features results in more than ten million combinations. It is impractical to perform this due to the computational burden. In the precious study, we adopted a sub-optimal method of genetic algorithm-based search, which is a stochastic search in the

feature space guided by the idea of inheriting, at each search step, good properties of the parent subsets found in previous steps [73]. Because of the large number of features, the convergence speed under GA was still very slow.

For the purpose of faster convergence and less risk of local minima, we proposed an approach of pre-feature selection to pre-select features having larger Bhattacharyya distance between two task conditions. The Bhattacharyya distance is the square of mean difference between two task conditions divided by the variance of the samples in two task conditions [74]. The Bhattacharyya distance was calculated on each feature (univariate) in feature pool indexing the feature separability between two task conditions, which was somewhat similar to ANOVA statistic test by evaluating the volume of the pooled covariance matrix of the class relative to the separation of their means. As Bhattacharyya distance indexes the separability directly, it is preferable for feature selection with comparison of other indexing methods, for example, the Fisher Score which indexes the similarity. The features were sorted in descending order according to their Bhattacharyya distance; the first 100 features were retained for subsequent multivariate feature selection.

Assuming that movement intention associated cortical activities occur over the motor cortex, we empirically reduced the channel number from 27 to 16, which covered both left and right motor areas (channels CZA, C3A, CZ, C1, C3, C5, CZP, C3P, PZ, P3, C4A, C2, C4, C6, C4P, P4). Furthermore, we extracted alpha and beta band (8–30 Hz) activities for modeling and classification. Consequently, the total number of extracted features was 8

(frequency bins) × 16 (channels) = 128 features. Bhattacharyya distance provides an index of feature separability for binary classification, which is proportional to the inter-class mean difference divided by intra-class variance [75]. The empirically extracted features were ranked by the Bhattacharyya distance for further classification.

2.4.2 Two-step modeling/classification

As Figure 5 shows, the first step was to identify whether the signal belonged to control commands (true positive or TP) or non-control commands (true negative or TN), as we wanted to keep false triggering / false positive rate (FPR) as low as possible and true positive rate (TPR) sufficiently high. For modeling using the calibration dataset, we first grouped all three active tasks ('GS', 'RT', 'LT') into one category as control signals, leaving 'ID' tasks as another category, i.e., non-control signals. We applied Mahalanobis linear distance (MLD) classifier to find the prototype centers of the two categories. For each sample in the training set, we calculated the distance between itself and each center and then took the difference $\Delta\vec{d}$ to finally get $\Delta\vec{d}$ for all the training samples. By applying a series of thresholds to separate $\Delta\vec{d}$, we could classify the samples under different accuracies, we then got the ROC plot [76] for all thresholds on testing samples. We selected an optimal threshold under which FPR was lower than 10% and TPR higher than 80%, or sub-optimal threshold which was close to the left upper corner of the ROC curve and applied that threshold in the online wheelchair control to separate Idle from Active.

If it was Idle, the computer did not send out any control command, instead, the wheelchair kept current moving; if classified to Active, the second step was a 3-class classification, to further determine whether it was a 'GS', 'LT' or 'RT' command. In each step, the features (power data extracted from T1 and T2 windows over different frequency bins and electrode locations) were ranked by the Bhattacharyya distance and the ones with higher ranks were used for classification by a MLD classifier.

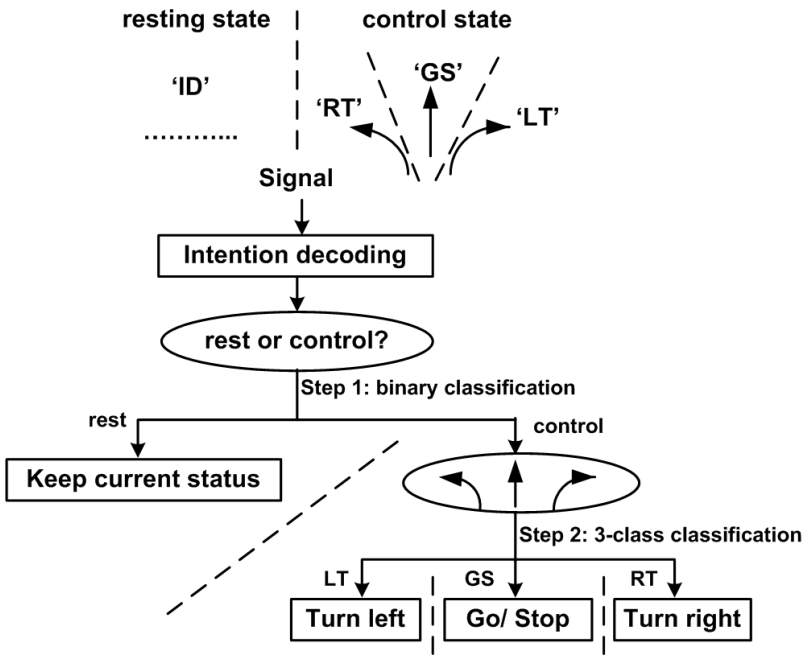

Figure 5. Demonstration for the two-step classification. Step 1 is a binary classifier, separating Idle from Active; Step 2 is 3-class classifier, further determine which Active command the sample belonged to.

2.5 Experimental results

Table 2 shows that except for S1 who quit due to sleepiness, the other four subjects who finished all physical and imagery sessions finally got 100% target hit rate in the second set of games (Game 2) with motor imagery, with time generally shorter than Game 1 (except for S4), due to fewer misdetections in Game 2. This shows that subjects became familiarized with the BCI operation and learnt to cooperate with the BCI system and improve their sense of kinesthetic imaginary. Notice that Game 2 in the physical session also took a shorter time than that in Game 1 ($t=5.03$, $df=39$, $p\text{-value}<0.001^*$), which can be considered evidence that the subjects started to learn.

Taking a closer look at the target reaching time in the second imaginary game, we found that 58.6s was the average time for subject 2,3,4 and 5 to reach a target 10m away. 5.9s/m reflected a reasonable speed for a wheelchair used by paralyzed patients [65].

Both binary and 3-class classification affected subjects' control performance; binary classification was of more importance as non-control states (Idle tasks) accounted for 46.9% of all tasks. This was in accordance with another study conducted by Pfurtscheller's group [77] where the subject "walked" straight in a virtual environment using two signals, IC (intentional control) and NC (non-control) in order to reach avatars. As they pointed the drawback of their design was that the subject was forced to stop at the avatar for a

minimum 1s NC period, but the actual subjects' stopping time was very short with the mean 0.47s, which means the false triggering (FP) was inevitable.

In our imaginary movement, no values for TP and FP can be given, for the same reason as the study mentioned above. Using their evaluation method, for S2, S3, S4, and S5, TPR in motor imagery would be 63/64=98.4% and missed hits (false negative rate/FNR) =1/64=1.6% (calculated from Table II); FP and true negative (TN) cannot be evaluated. However, since target reaching time for motor imagery was comparable to that for physical movement, we can calculate TPR and FPR (shown in Figure 6) by monitoring the EMG activity in physical movement.

Table 2. Hit rate and average target hit duration in each game

Hit rate (%) & Duration (s)	physical		imaginary	
	Game1(8runs)	Game2(8runs)	Game 1(8runs)	Game 2 (8runs)
S1	100 (85.8)	87.5 (52.0)	*	*
S2	100 (40.8)	100 (34.8)	100 (43.0)	100 (41.5)
S3	100 (63.3)	100 (63.0)	100 (59.5)	100 (39.5)
S4	87.5 (67.0)	100 (58.0)	87.5 (70.9)	100 (88.0)
S5	100 (50.5)	100 (49.8)	100 (75.3)	100 (65.5)

TPR is the sensitivity, indicating the active command recognition rate. For all subjects, TPR ranged from 64.3% to 100% (mean 84.3%) which was much higher than chance value

53.1% (percentage of active command). FPR is the false triggering rate ranging from 3.8% to 43.5% (mean 19.0%) which means specificity (TNR or 1-FPR) was much higher than chance value 53.1% (percentage of active command). FPR is the false triggering rate ranging from 3.8% to 43.5% (mean 19.0%) which means specificity (TNR or 1-FPR) was 81.0%, much higher than chance value 1-53.1% or 46.9%.

For physical movement, average target hit time was 56.5s, obtained from Table 2. With the calculation above, one run took about 9.5 commands to hit the target, about 0.89 Idle was detected as active (1 false triggering) and (5.31-4.48=0.83) active commands were detected as Idle (1 insensitivity). This calculation gave us a general idea for motor imagery control which took an average 60.4s for each target hitting. Under this detection rate, subjects reported good sense of control.

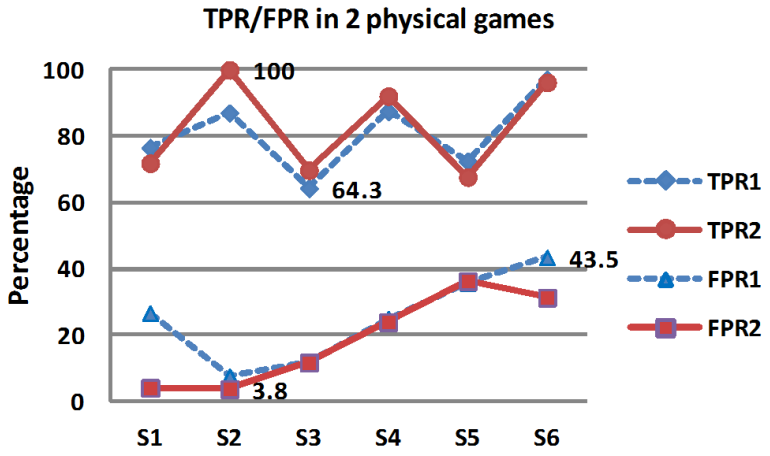

Figure 6. True positive rate (TPR or active command recognition rate), and false positive rate (FPR or the ratio of 'Idle' command recognized as active command) for all subjects in two physical games.

Figure 7 shows the traces for all the games in physical and imaginary sessions for each subject. We can see that S2, with several hours' previous exposure to other BCI studies, was more comfortable than the other subjects even from the first run and also displayed good performance in motor imagery. S3, although a naive BCI user, caught up very quickly and over performed S2 in the last motor imagery game.

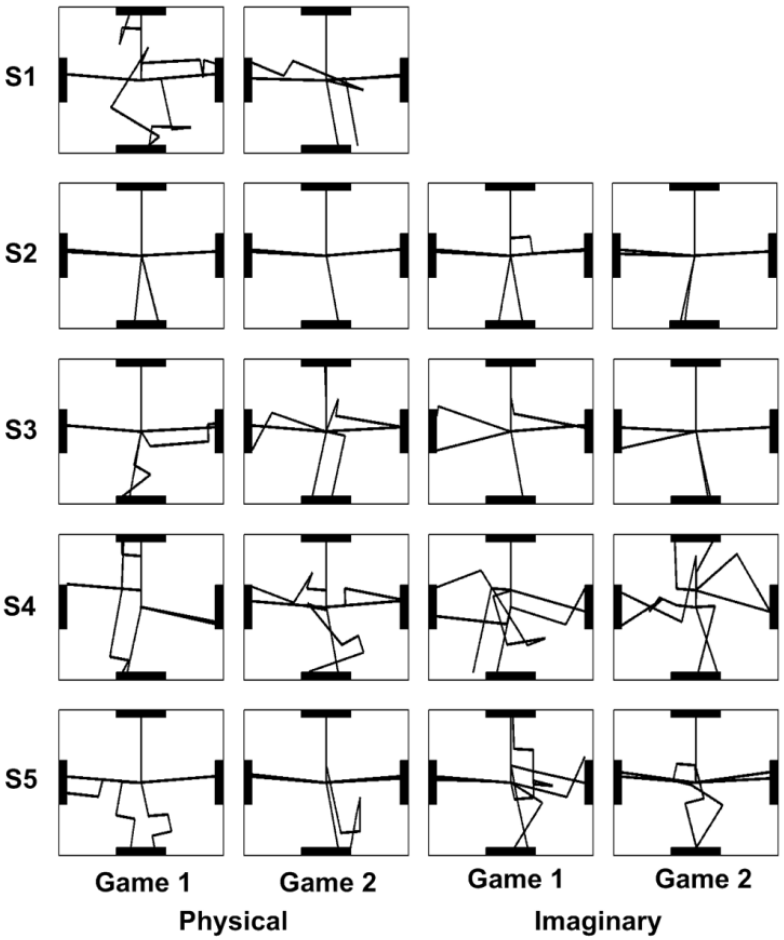

Figure 7. Traces of all physical and motor imagery games for each subject. Each game had eight runs/target reaching.

Table 3 shows the best EEG features used for each subject in physical and binary wheelchair control games, in terms of electrodes and frequency bins (4Hz bin width). We notice that frequency bins for binary classification more often appeared in alpha and lower beta bands (bin 3-6 or 9-24Hz); for 3-class classification, bin 7 and 8 (25-32Hz) were involved more often. This proved the fact that for 3-class classification, ERS, which occurred mostly in beta band, played a significant role. The best channels for binary classification more often appeared in C3 and C4; for 3-class classification, channel C1 and C2 were also involved for some subjects, which may indicate that ERS in central motor area was stronger for some subjects and its contrast with ERD contributed much in discrimination of GS/RT/LT.

Figure 8 is an illustration showing the ERD/ERS of S2 and S3 in motor imagery. Best electrodes were selected (C3 and C4 for S2, C1 and C4 for S3). As can be seen, during the Idle state, subjects thought about nothing, baseline activity exhibited throughout all frequency bands. In 0-1.5s of the active tasks where subjects imagined wrist extensions, ERD (blue) occurred most of the time, at around 10-20Hz frequency band, bilaterally distributed. During 1.5-4s, subjects either continued imagined movement where ERD still sustained or stopped motor imagery where ERS (red) showed up. ERS occurred mainly on the contralateral hemisphere. For S3, ERS appeared at higher frequency band than S2, and more towards central electrodes. From the plots we can see that the spatial and and

temporal EEG signal differences among different motor tasks can be reflected from ERD/ ERS patterns associated with movement intention which can be decoded by analyzing the data in T1 and T2 time windows.

Table 3. EEG features (specific frequency bins at specific electrodes) that were used for binary classification (Idle/Active) and 3-class classification (GS/RT/LT) in physical /motor imagery session for each user

	Electrode (frequency bin)			
	Physical		Imaginary	
User	Binary	3-class	Binary	3-class
S1	C3,C4	C3,C4	C3,C4	C3,C4
	(5,6)	(5,6)	(4,5)	(4,5)
S2	C3	C3,C4	C3	C3,C4
	(5,6)	(4,5)	(5,6)	(3,4)
S3	C3,C4	C1,C3	C3,C4	C1,C3
	(6,7)	(7,8)	(4,5)	(7,8)
S4	C3,C3P	C3,C4	C3,C3P	C3,C4
	(5,6)	(6,7,8)	(4,5)	(6,7)
S5	C3,C4	C1,C4	C3,C4	C1,C2
	(4,5)	(6,7,8)	(4,5)	(7,8)

To answer why involving ERS as opposed to ERD could potentially enhance detection accuracy, we need to quantitatively examine ERD/ ERS in the three mental tasks. Figure 9 shows ERD/ERS values at C3 and C4 for S2-S5 in physical movement (top two) and imagined movement (bottom two), under the left turn (LT), right turn (RT) or Go/Stop (GS) tasks. The left side describes the T1 window and right side describes the T2 window.

First, it is obvious that ERD/ERS power distribution in the physical and motor imagery sessions is quite similar, except that power in motor imagery session is much weaker than that in physical session, which is consistent with our previous reports. Second, as we can see in the T1 window (Figure 7), for all three tasks, both C3 and C4 generally exhibit negative values because of the bilateral ERD distribution during left/right hand (imagined) movement. Conventional rhythmic regulation is largely based on an ERD approach, however, due to the fact that ERD could be difficult to be detected from baseline because of the variance and the similarity that exists among different mental tasks (p-value=0.8227 for physical and p-value=0.5207 for motor imagery), intensive training may be necessary before stable control could be attained.

In contrast, the proposed novel design makes the most of spatial and temporal difference of EEG features during mental tasks, as it involves spatially focal ERS associated with cessation of mental tasks in the T2 window, which essentially enhances the difference among mental tasks. As can be seen in the T2 window, positive power values generally exhibit on the contralateral hemisphere for RT and LT tasks while, in contrast, negative power values bilaterally exhibit for GS tasks. Three tasks can be classified easily in the physical session (p-value=0.0002*) and less easily in the motor imagery session (p-value=0.0856).

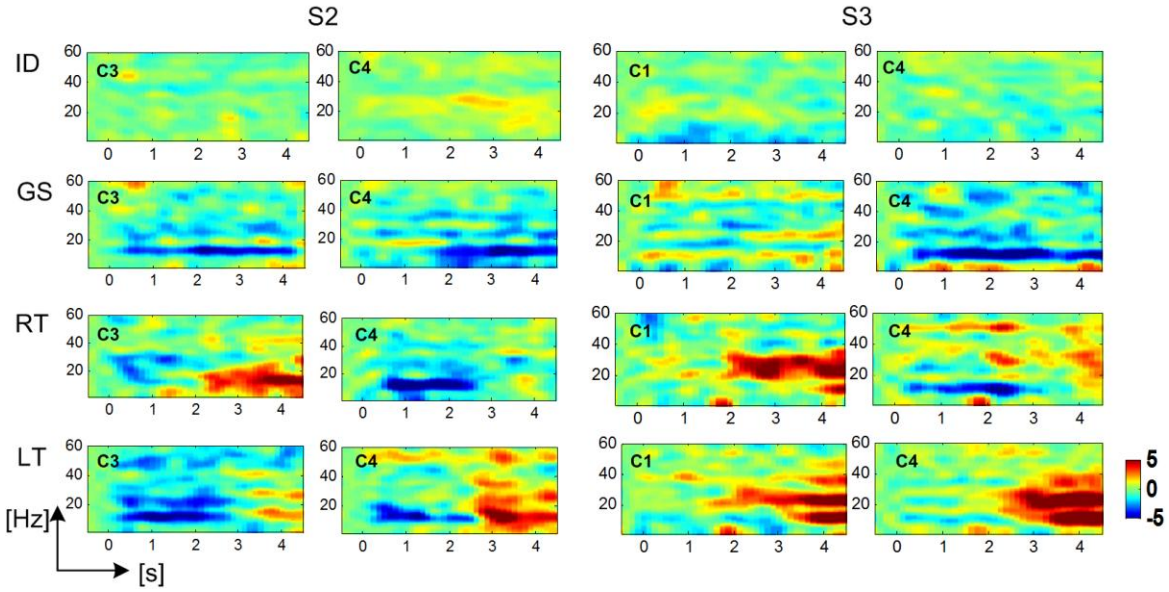

Figure 8. Illustration of time-frequency plots for S2 and S3 in motor imagery tasks. X axis represents time. Specifically, in non-Idle tasks, from 0-1.5s subjects performed imagined right wrist extension (GS/RT) or left wrist extension (LT) and from 1.5s-4s, either continued imagined extension (GS) or stopped and relaxed (RT/LT). Y axis indicates frequency. Red means power increase and blue is power decrease, with green the baseline.

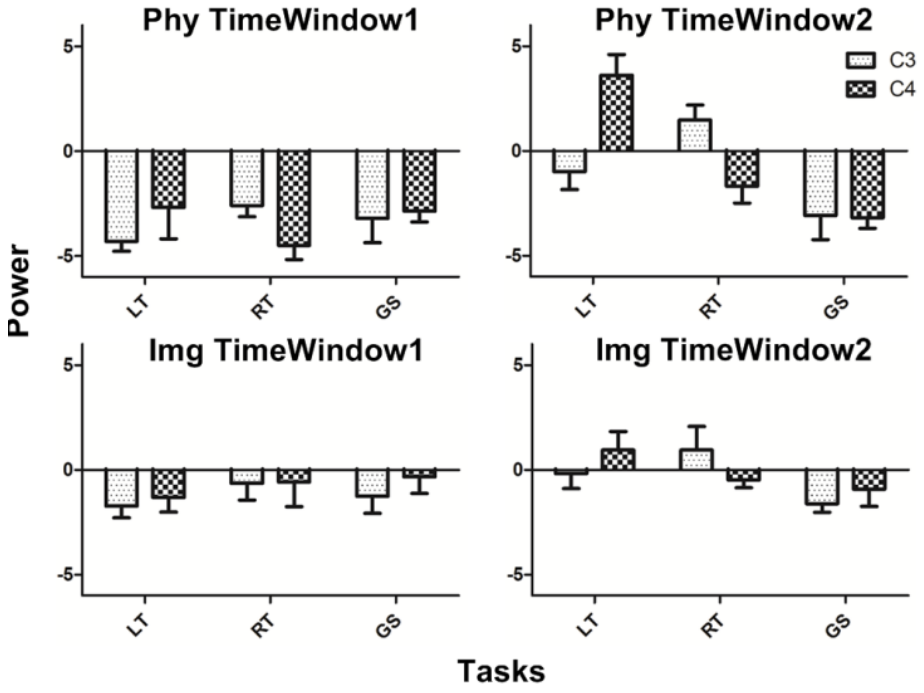

Figure 9. ERD/ERS amplitude at C3 and C4 for subject S2-S5 in physical movement (top two) and imagined movement (bottom two). Left side describes T1 window and right side describes T2 window

For each subject, the best electrode locations and frequency bins used for control signals were provided by Bhattacharyya distance. Figure 10 is an example where Bhattacharyya distance was used in binary classification to separate active tasks from Idle. One of the best frequency bins were selected to illustrate each subject's performance. As subjects exhibited variant performances in motor tasks, we usually selected two or three major channels/frequency bins for each subject as the best ones. As can be seen, S2 was more familiar with BCI than the other three, and therefore the pattern was more stable (less noisy in the surrounding electrodes) than others. Compared with S2, S3 had the best electrodes more focal, evenly on both hemispheres. S4 had C3 and C3P both on the left hemisphere, as the best electrodes for binary classification and S5 had a few ideal electrodes providing good separability, similar with S2.

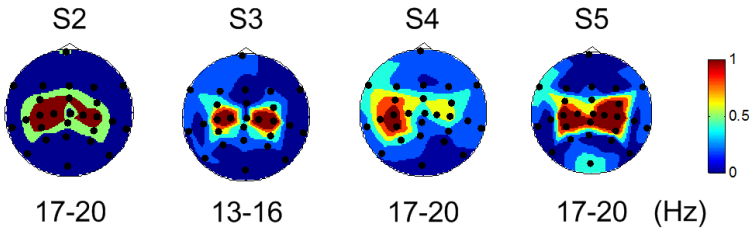

Figure 10. Head topography plots of Bhattacharyya distance for binary discrimination for the 4 subjects in motor imagery tasks. Dark red areas indicate highly distinguishable and dark blue means the opposite. Best frequency bins and channels for each subject differ.

2.6 Discussion

In this study, we have presented an effective and practical paradigm of a continuous EEG-based BCI for virtual wheelchair control of subjects in their first visit. The wheelchair could be operated to turn left or right, to go straight or stop, with all the basic motion functions that a real wheelchair has. The prominent induced power decrease (ERD) and power increase (ERS) associated with imagined natural movements allowed the reliable discrimination of movement intentions, and therefore improved control accuracy and increased the degrees of freedom of the wheelchair control system. The result showed that a high hit rate (87.5%-100%) could be achieved by controlling the simulated wheelchair continuously moving in a 2-D plane when subjects imagined hands' movements. It should be noted that subjects achieved the reasonable control performance in their first visits.

Compromise is always needed when optimizing control accuracy and speed. While control accuracy is satisfying, increasing the wheelchair's movement and rotation speed is also of key interest. As we have noticed, it took time for the correction of wheelchair overshoot which can be observed in Figure 6 from the sharp turn of the trajectories. This was caused by the unresponsive detection periods T1 and T2. However, as T1 and T2 are essential for ERD and ERS to happen, they are indispensable for the proposed strategy. Thus, to optimize the length of the detection window to make a more flexible, yet reliable wheelchair control is our next step.

Moreover, reduction of the number of electrodes could be performed with the expectation of comparable results, as we found through analysis that subjects exhibited stable features in several electrodes, namely C1-C4, and occasionally C3P and C4P. Fewer electrodes would reduce setup time and undoubtedly will aid the spirit of the subjects. As this was the subjects' first visit, we asked them to perform physical movement first. On one hand, it allowed us to examine their movement execution and ERD/ERS features before motor imagery and on the other hand it allowed them to find the right way to perform motor imagery tasks.

EMG contamination from facial muscles may possibly cause serious problems in BCI development [78]. Throughout the experiment, EMG signal was monitored for all subjects, to make sure correct movements were performed and no EMG occurred during motor imagery. Further, feature analysis showed that beta activities restricted to motor areas were used for classification. Therefore, EMG contamination was not a concern in this study.

Compared with our previous study where users performed step by step discrete 2-D cursor control, which is stable but slow, the current study is taking a major step forward in trying to apply the rationale to wheelchair control, by involving non-control state and continuous control strategy as a part of our user friendly design. Specifically, subjects imagined human natural hand movements. Imagined left hand movement in T1 window sent out

control command for left turn; imagined right hand movement in T1 window sent out control command for right turn; imagined right hand movement in both T1 and T2 window sent out Go/Stop command. It is in a manner similar to driving, when people want to start the engine, finish turning and go straight, or stop during emergency, they step firmly on the accelerator or brake for a period. Drivers hold this state when they don't want to change direction or stop, which is similar to the non-control state in this study where subject remained relaxed. This gave subjects 2-4.5s intervals between two active commands which allowed them to take a break and get prepared for the next movement. For the condition that they kept moving/ turning, the non-control state allowed even longer relaxation time for the subjects, or for the potential paralyzed patients. The current design aimed at ease of use for the potential user while keeping a reliable sense of control, with good control speed.

Another aspect of user friendly design is that the paradigm fixed the initial facing direction of the wheelchair upwards in each run while changing target directions, in order to mimic the real world target reaching tasks, where users may need to turn the wheelchair by different angles and then move forward. In the typical setting as we did here: moving forward, turning left/ right and to the opposite directions, we had a good chance of examining all combinations of commands, such as non-control & control, move forward & stop, turn & move forward, just as in real wheelchair control or car operation. Yet, the current virtual wheelchair design is adopted to be most user friendly in a virtual scenario. Once the approach is fully validated and the system performance is optimized in a virtual

environment, the next step of the experiment will be taken. Before a real wheelchair can be finally incorporated into the system, integration issues should be carefully considered and simulated, parameters such as mechanical system delay and emergency control, for example fault tolerant strategy, will be examined.

Considering that subjects achieved comparable performances as S2 who had several hours of previous BCI experience, we expect that they would improve their control skills quickly in later studies. Compared to the current EEG-based continuous 2-D BCIs that require months of subject training and may cause fatigue in the long run, the proposed BCI system exhibited prominent advantages. In brief, the results proved the feasibility of the ERD/ERS based brain-controlled virtual wheelchair system, which subjects could rapidly attain a significant level of control with a short calibration period. In the future research, we would consider how to develop asynchronous wheelchair control based on the current system to further increase control speed while maintaining reasonable control accuracy.

CHAPTER 3

Exploration of classification methods

3.1 Software and toolbox for classification exploration

The implementation and visualization of feature selection and classification was done in Matlab and Weka, and statistical evaluation was done in JMP. The simulation was implemented in programming language C++, by our collaborators at the Mechanical Department at Huazhong University of Science and Technology, China. The aim of the simulation on one hand was to investigate a human-robot cooperative strategy based on our 2D wheelchair control rationale with robotic intelligent controls, which would be incorporated into our system to reduce the demand of the human users; and on the other hand, by using different EEG decoding accuracies as input, its simulation results provided control accuracies of wheelchair in different scenarios as output, which, as a feedback, set the requirement to our decoding system.

3.2 EEG signals to be classified

As in the 2D virtual wheelchair control study, the four types of EEG signals, using their corresponding command name i.e. ID, LT, RT and GS were studied here. All the data were obtained in that study through performing physical or imaginary of hand movement tasks. Before we explored pattern recognition techniques to classify them, a simulation was

performed using the four signals as input to a human-wheelchair cooperation system with intelligent control. Pass-door test and positioning test were done under scenes with/without obstacles, and target hit rates were obtained (Table 4-7).

Table 4 Hit rate of pass-door tests in the scene with no obstacles.

Hit Rate		Accuracy of *None-ID* signals				
		0.6	0.7	0.8	0.9	1
Accuracy of *ID* signal	0.6	0.7	0.95	1	1	1
	0.7	0.95	0.95	1	1	1
	0.8	0.85	1	1	1	1
	0.9	0.9	1	1	1	1
	1	1	1	1	1	1

Table 5 Hit rate of pass-door tests in the scene with 10 obstacles.

Hit Rate		Accuracy of *None-ID* signals				
		0.6	0.7	0.8	0.9	1
Accuracy of *ID* signal	0.6	0.6	1	1	1	1
	0.7	0.8	1	1	1	1
	0.8	0.8	1	1	1	1
	0.9	0.95	0.95	1	1	1
	1	0.9	1	1	1	1

Table 6 Hit rate of positioning tests in the scene with no obstacles.

Hit Rate		Accuracy of *None-ID* signals				
		0.6	0.7	0.8	0.9	1
Accuracy of *ID* signal	0.6	0.63	0.77	0.83	1	0.97
	0.7	0.6	0.83	0.93	0.97	0.97
	0.8	0.6	0.77	0.9	1	1
	0.9	0.77	0.83	0.9	1	1
	1	0.63	0.87	0.9	1	1

Table 7 Hit rate of positioning tests in the scene with 10 obstacles.

Hit Rate		Accuracy of *None-ID* signals				
		0.6	0.7	0.8	0.9	1
Accuracy of *ID* signal	0.6	0.55	0.75	0.9	1	1
	0.7	0.55	0.75	0.85	1	1
	0.8	0.45	0.75	1	1	1
	0.9	0.7	0.7	0.8	0.95	1
	1	0.5	0.95	0.9	1	1

From the results we can see that when the decoding accuracy for ID was higher than 0.6 and for Non-ID was higher than 0.7 (0.8), relatively high success rate 95% (80%) for pass-door test (positioning test) could be obtained under scenes with or without 10 obstacles.

In this case, to get the hit rate generally above 80%, our classifiers output needs to satisfy that ID accuracy is above 60% and Non-ID accuracy is above 80%. In order to further enhance the success rate of the brain-controlled wheelchair in navigation and positioning

tasks, optimization of EEG decoding can be done according to different application environment. If the actual application is mainly long distance navigation, where more ID signals are needed in the command sequence and more relaxed the users are, the ID accuracy should be ensured as priority. If most applications are limited in the limited interior space, and need positioning more often, the Non-ID decoding accuracies should be ensured first, to guarantee accurate turning or Go/Stop decoding.

3.3 Exploration of classification methods

3.3.1 One-vs-All logistic regression

Logistic regression attempts to model the probability of a binary outcome using a linear function of the predictors. In this study, we used multiple one-vs-all logistic regression models to build a multi-class classifier. Since there were 4 classes, we trained 4 separate logistic regression classifiers. Figure 11 gives the scheme for the one-vs-all classification method. Concretely, the 4 classifiers would be binary ones ID-vs-Non-ID, RT-vs-Non-RT, LT-vs-Non-LT and GS-vs-Non-GS. After training the classifier, we used it to predict new data in a testing dataset. For each input, we computed the "probability" that it belonged to each class. The one-vs-all prediction function would pick the class for which the corresponding logistic regression classifier output the highest probability and returned the class label (1, 2, 3 or 4) as the prediction for the input data.

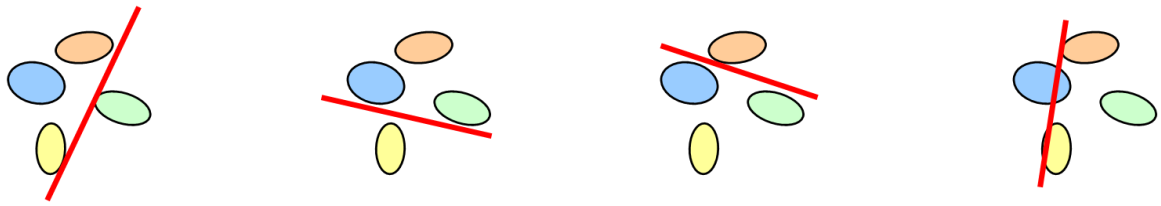

Figure 11. Scheme for One-vs-All classification method

For the logistic regression, hypothesis is defined as: $h_\theta(x) = g(\theta^T x)$, where function g is the sigmoid function, defined as: $g(z) = \frac{1}{1+e^{-z}}$. The training process is for a set of training data (x^i, y^i), we want to find a set of θ (coefficients of features) that can minimize the cost function, which is:

$$J(\theta) = \frac{1}{m}\sum_{m}^{i=1}[-y^i \log(h_\theta(x^i)) - (1-y^i)\log(1-h_\theta(x^i))]$$

As in some cases, number of training data m could be much smaller than the number of features, so that the learnt hypothesis may fit training set very well where $J(\theta) \approx 0$, but it fails to generalize to the new samples. To overcome this over-fitting problem, we add a regularization term $\frac{\lambda}{2m}\sum_{j=1}^{n}\theta_j^2$ into the cost function. By adjusting the parameter λ, we penalize the learning algorithm and keep θ_j small to ensure that each feature contribute a bit to predicting y.

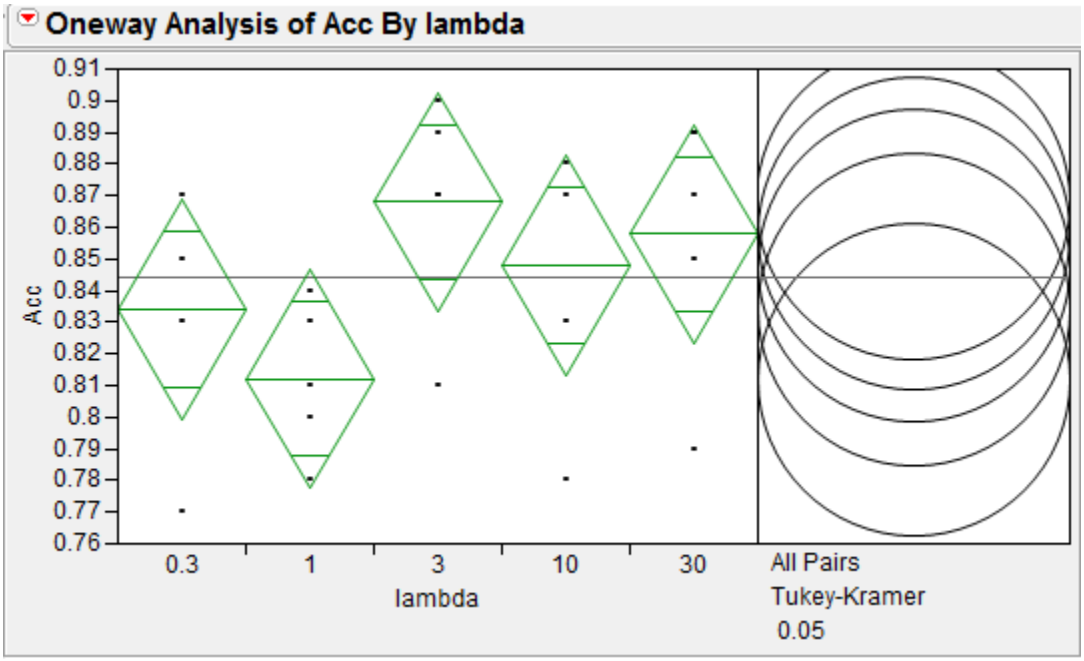

Figure 12. Oneway Anova analysis of the affects of different λ on physical data of 5 subjects.

We applied this classifier on all the physical data of the 5 subjects separately. Input data has 2*7*16=224 features (2 time windows, 7 frequency bins and 16 electrodes), and number of data for each subject ranged from 192 to 288. Each time we selected λ to be one of the numbers 0.3, 1, 3, 10, and 30. 10-fold cross validation was used to evaluate the performance of the classifier on each subject individually. From Figure 12 we can see that $\lambda = 3$ gave the highest average testing accuracy 86.8%, although no statistically significant difference existed among the results of this set of λ (p-value=0.18). Using $\lambda = 3$ on each subject's physical data, we got the accuracy ranging from 80.6% to 90.0%. Considering the requirements set by the simulation study, this classification accuracy is acceptable as it's above 80%.

As the previous steps were taken separately for each subject, it's interesting to see whether we could pool all the subjects' data together, and then apply classifications on the pooled data, in order to see how the classifier generalizes so that it may help to build a general model for classifying new subjects' data. If this is the case, it could save much time of getting a lot of data from the same individual.

Learning curve is helpful in debugging learning algorithm. It plots training and cross validation error as a function of training set size. Figure 13 shows the learning curve which is created by using the pooled physical data of all the subjects when λ is set to 3. As can be seen, as more training data are used, cross validation accuracy error is reduced more and gets closer to training error. Since there is no gap between training error and cross validation error, the classifier is over-fitting free. When the number of training examples approaches about 200, both training and cross validation come to a plateau of error equals 0.2 which is a sufficiently small number. So, the classifier is not suffering from high bias either, which means the model fits the data well as long as samples for training get above 200.

When the number of training is less than 200, training and cross validation error has bigger gap, which means the classifier could over-fit the training data. This is usually the case as

we normally could only get 100-200 data samples from each subject in a single visit (2 out of 5 subjects got more than 200 samples of physical data in this study). So, if we want to build robust classifiers with less data, we may choose to select a smaller set of features or increase the over-fitting penalty parameter λ.

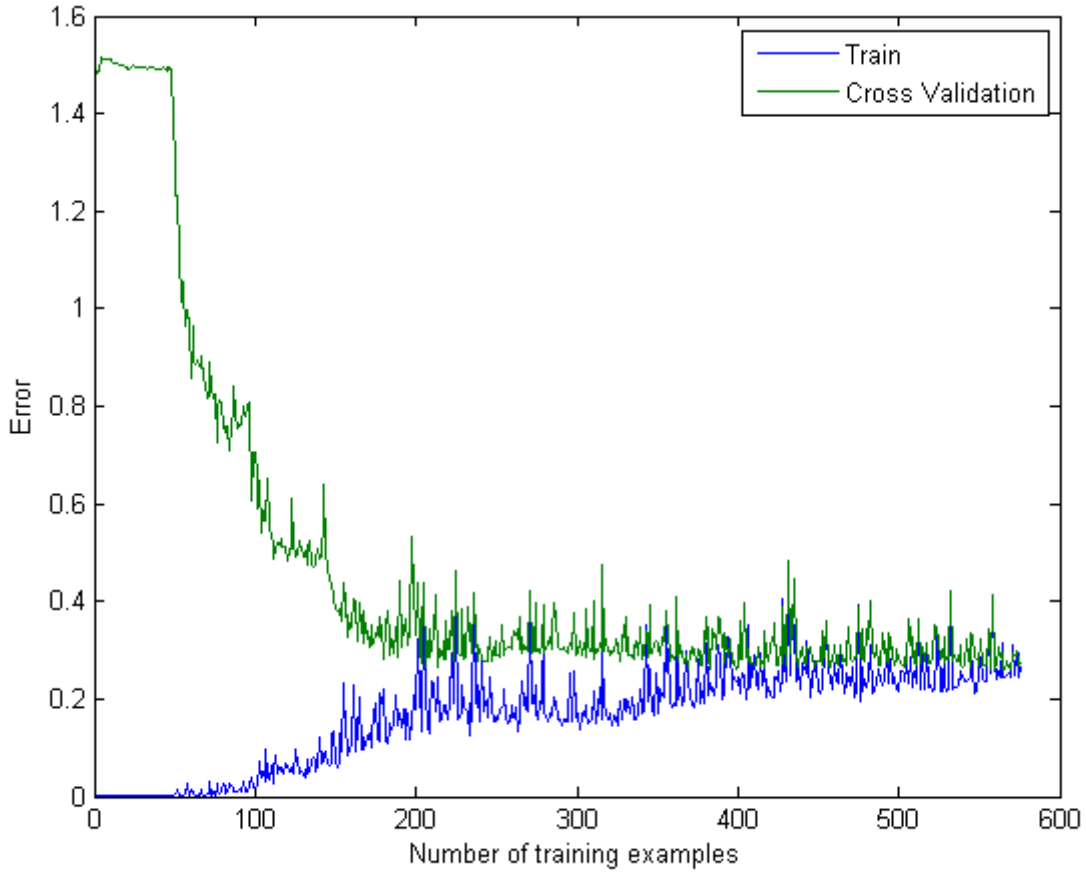

Figure 13. Learning curve for the logistic regression using physical data.

As 4 subjects participated in imaginary movement, we applied this classifier on all the imaginary data. Features kept the same as those in physical test. Each time we selected λ to

be one of the numbers 0.3, 1, 3, 10, and 30. 10-fold cross validation was used to evaluate the performance of the classifier. From figure 14 we can see that $\lambda = 1$ gave the highest average testing accuracy 79.8%, and also there is no significant difference among the results of this set of λ (p-value=0.98). Using $\lambda = 1$ on each subject's imaginary data, we got the accuracy ranging from 65% to 89.2%.

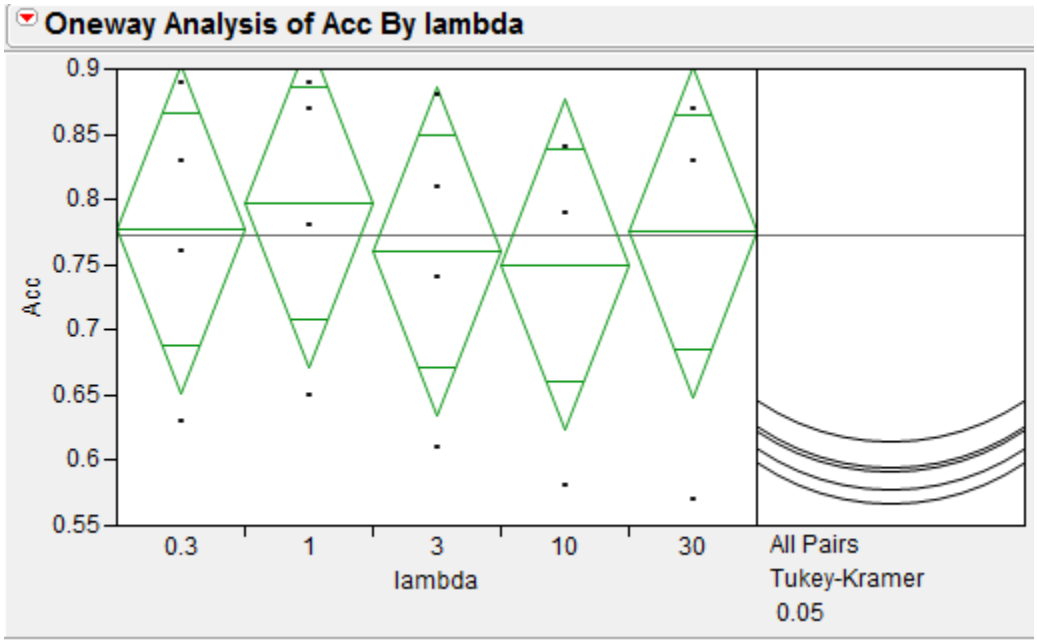

Figure 14. Oneway Anova analysis of the affects of different λ on imaginary data of 4 subjects.

3.3.2 Support vector machine classifier

Support vector machine (SVM) is a representation of the examples as points in space, mapped so that the examples of the separate categories are divided by a clear gap that is as

wide as possible (Figure 15). New examples are then mapped into that same space and predicted to belong to a category based on which side of the gap they fall on.

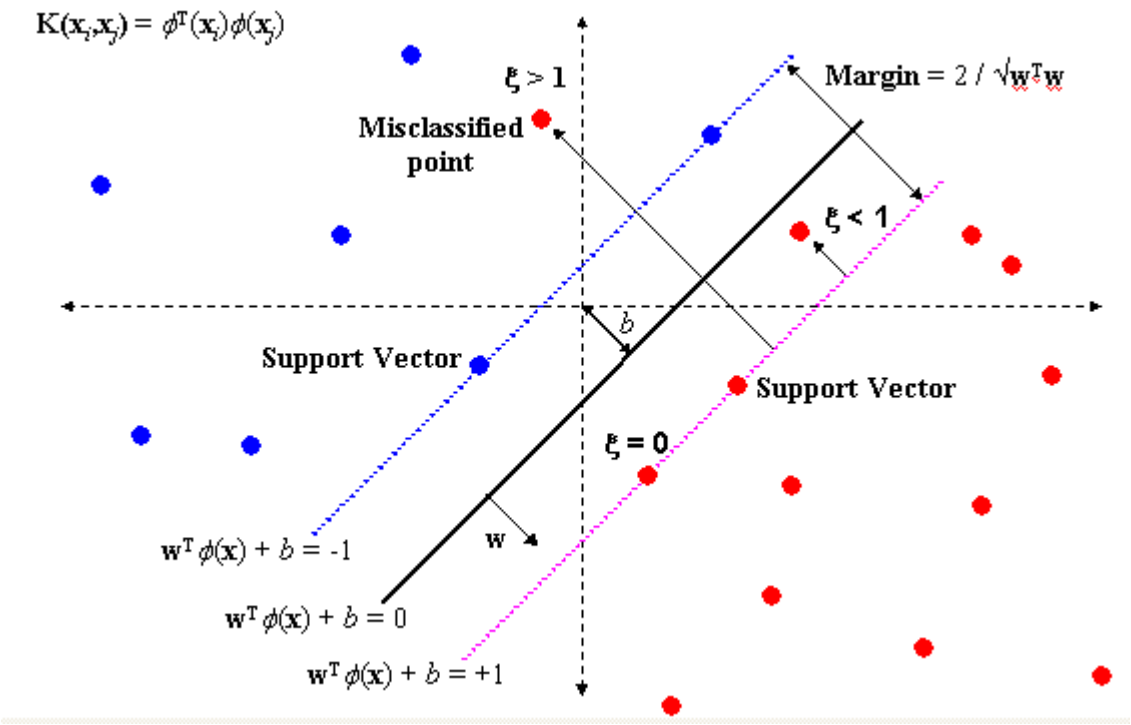

Figure 15. The SVM learns a hyperplane which best separates the two classes (indicated by red dots and blue dots).

Given a training set of instance-label pairs (x_i, y_i), $i = 1 \ldots l$ where $x_i \epsilon R^n$ and $y \epsilon \{1, -1\}^l$, the SVMs require the solution of the following optimization problem:

$$\min_{w,\xi,b} \frac{1}{2} w^T w + C \sum_{i=1}^{l} \xi_i$$

$$\text{Subject to} \quad y_i(w^T \phi(x_i) + b) \geq 1 - \xi_i,$$

$$\xi_i \geq 0.$$

Where $K(x_i, x_j) = x_i^T x_j$.

Here training vectors x_i are mapped into a higher (maybe infinite) dimensional space by the function ϕ. SVM finds a linear separating hyperplane with the maximal margin in this higher dimensional space. C > 0 is the penalty parameter of the error term. Furthermore, $K(x_i, x_j) = \phi(x_i)^{\mathrm{T}}\phi(\mathrm{x_j})$ is called the kernel function.

We choose Gaussian function to be used as the radial basis (RBF) function (Figure 16). The RBF kernel is written as: $K(x_i, x_j) = e^{-\gamma\|x_i - x_j\|^2}$. The output of the kernel is dependent on the Euclidean distance of x_j from x_i (one of these is the support vector and the other is the testing data point). The support vector is the centre of the RBF and γ determines the area of influence this support vector has over the data space. A smaller value of γ gives a smoother decision surface and more regular decision boundary. This is because an RBF with smaller γ allows a support vector to have a strong influence over a larger area. A smaller γ also reduces the number of support vectors. Since each support vector can cover a larger space, fewer are needed to define a boundary.

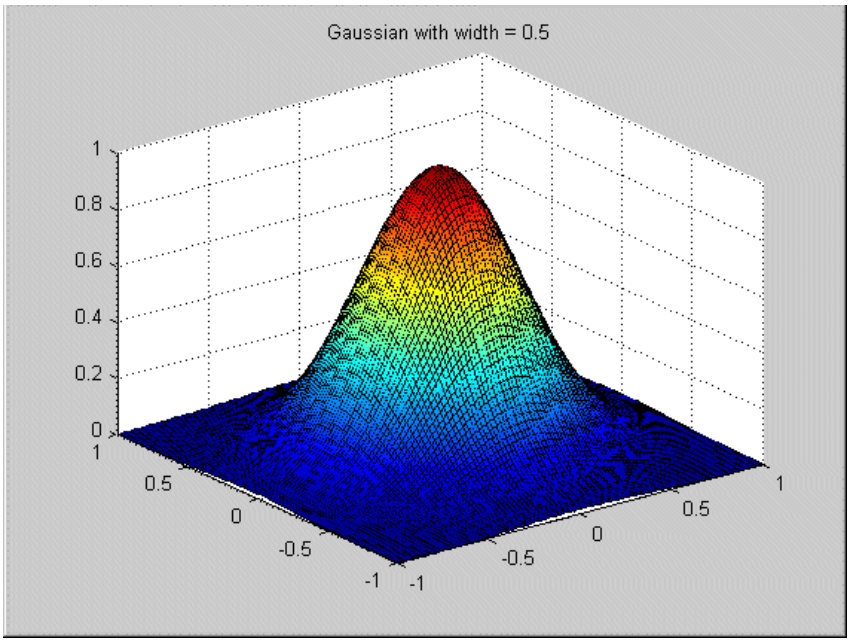

Figure 16. The Gaussian Radial Basis Function kernel.

In general, the RBF kernel is a reasonable first choice compared with other kernels. This kernel nonlinearly maps samples into a higher dimensional space so it, unlike the linear kernel, can handle the case when the relation between class labels and attributes is nonlinear. Furthermore, the linear kernel is a special case of RBF since the linear kernel with a penalty parameter C has the same performance as the RBF kernel with some parameters (C,γ). The second reason is the number of hyper-parameters influences the complexity of model selection. The polynomial kernel has more hyper-parameters than the RBF kernel.

We follow six steps to optimize the SVM classifier.

- Prepare data sets to fit the format of the LibSVM package.

- Conduct simple feature scaling on the data.
- Choose Gaussian RBF kernel.
- Use cross-validation to find the best parameter C and γ
- Use the best parameter C and γ to train the whole training set
- Test

Before applying SVM, feature scaling is very important. The main advantage of scaling is to avoid attributes in greater numeric ranges dominating those in smaller numeric ranges. Another advantage is to avoid numerical difficulties during the calculation. Because kernel values usually depend on the inner products of feature vectors, e.g. the linear kernel and the polynomial kernel, large attribute values might cause numerical problems. Figure 17 gives an example of feature scaling, where data on all feature space were scaled to fall in [0,1].

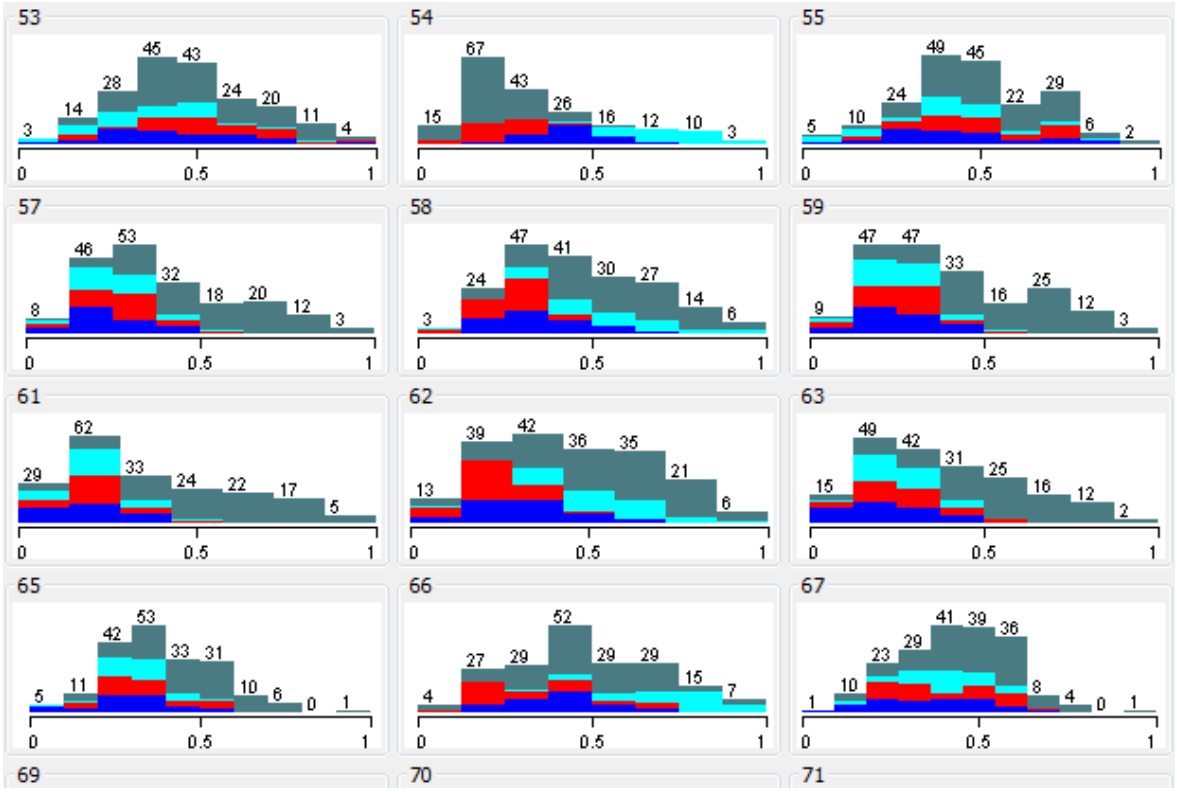

Figure 17. Illustration of feature scaling. Data on all the features were scaled to [0, 1].

We applied a "grid-search" on C and γ using cross-validation on 576 training data. Various pairs of (C, γ) values are tried and the one with the best cross-validation accuracy is picked. We tried exponentially growing sequences of C and γ, which is a practical method to identify good parameters. The grid-search is straightforward and can be easily parallelized because each (C, γ) is independent. Since doing a complete grid-search is still time-consuming, we used a coarse grid first. In this case, we tried C = 2^{-5}, 2^{-3}, 2^{-1}, 2^{1} , 2^{3}……2^{15} and γ = 2^{-15}, 2^{-13}, 2^{-11},……2^{5}., Figure 18 shows the result, as we can see the best C is around 2^{5} and the best γ is around 2^{-3} and the highest classification accuracy is 84.4%.

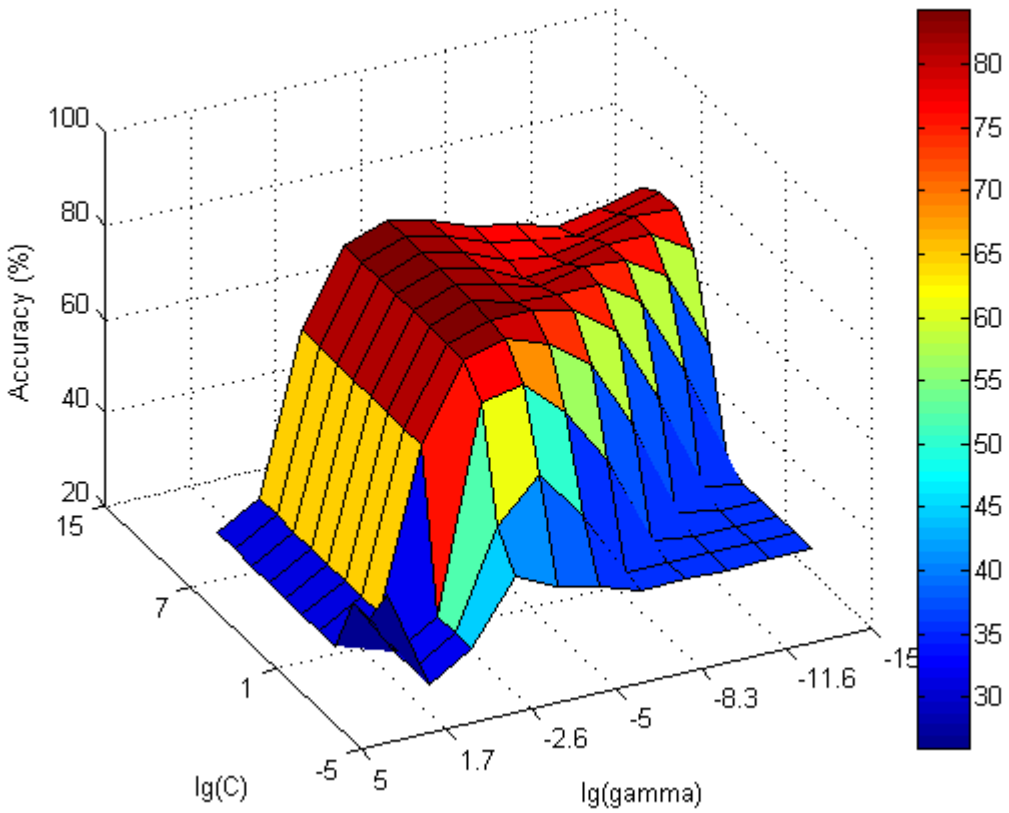

Figure 18. Loosed grid search on C = 2^{-5}, 2^{-3}, ……2^{15} and γ = 2^{-15}, 2^{-13},……2^{5}

After identifying a "better" region on the grid, a finer grid search on that region was conducted. We chose C=2^{4}, $2^{4.25}$, $2^{4.5}$, $2^{4.75}$, 2^{5} and γ=2^{-4}, $2^{-3.5}$, $2^{-3.25}$, $2^{-3.1}$, $2^{-3.05}$, 2^{-3}. Figure 19 shows the contour plot of the fine tuned result, and we found that the best pair of C and γ is C= $2^{4.5}$ and γ =2^{-3}.

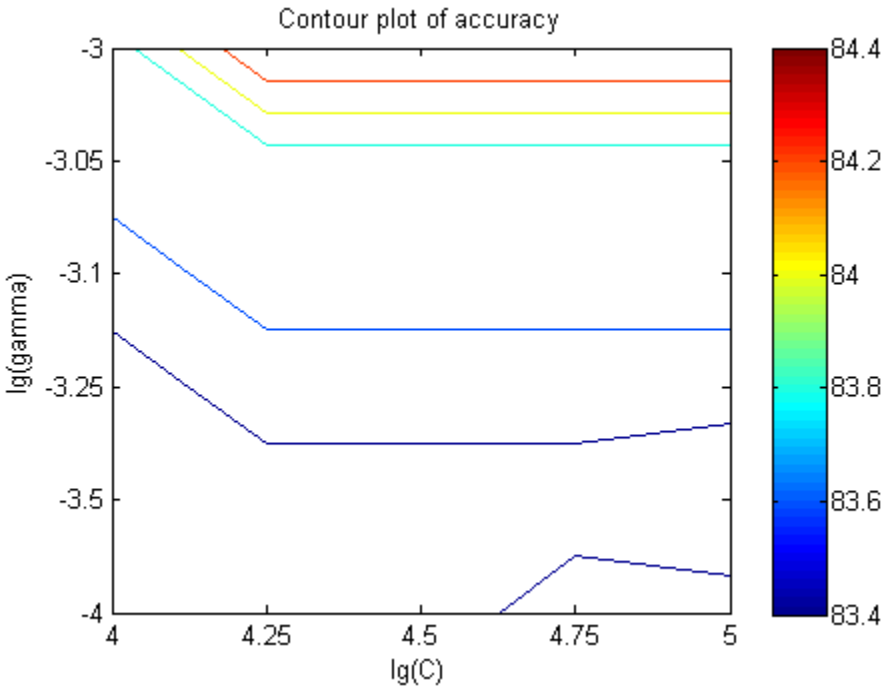

Figure 19. Fine grid search on C=2^{4}, $2^{4.25}$, $2^{4.5}$, $2^{4.75}$, 2^{5} and γ=2^{-4}, $2^{-3.5}$, $2^{-3.25}$, $2^{-3.1}$, $2^{-3.05}$, 2^{-3}

Figure 20 shows how exactly the 4 classes of data were classified correctly and incorrectly. Blue, red, green and light blue indicated GS, LT, RT and ID class respectively, and shape star means correct classification while square means incorrect classification.

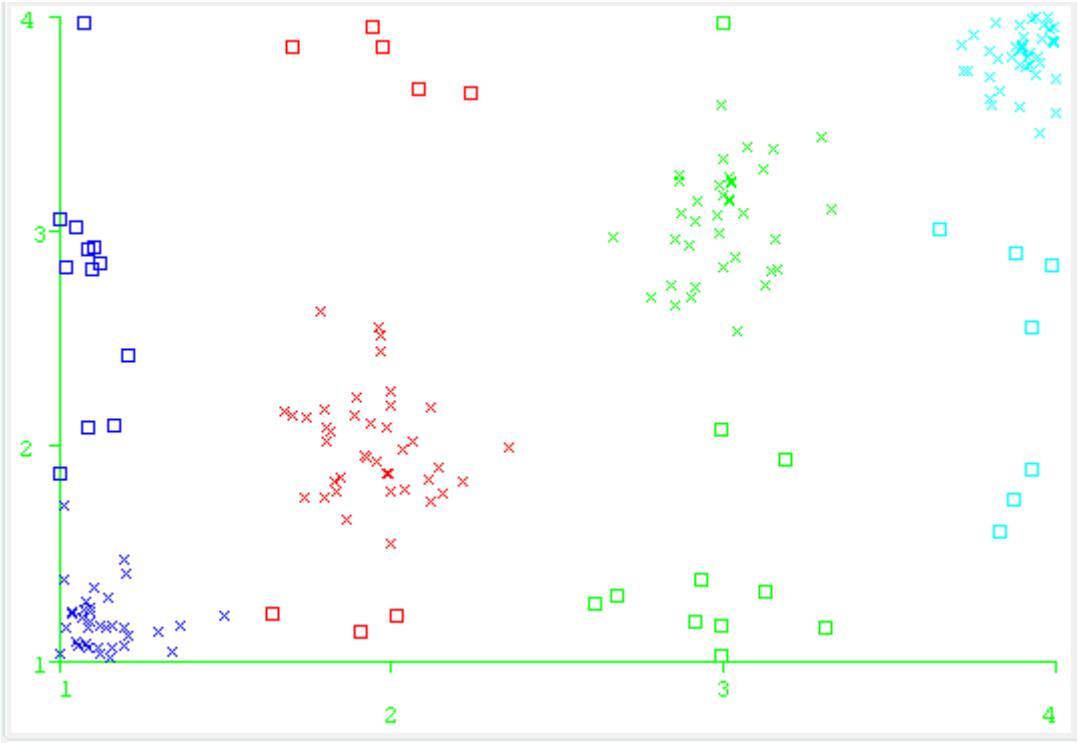

Figure 20. SVM testing result with the best trained C and γ.

We tried to see how it performed on classifying each subject's data by applying the parameter separately on each individual's dataset, and we got the accuracy ranging from 84.4% to 92.4% with the mean of 86.6%. Figure 21 gives an example of SVM classification output on a cross validation set. Class a, b, c, d represents for 'GS', 'RT', 'LT', and 'ID'.

```
=== Stratified cross-validation ===
=== Summary ===

Correctly Classified Instances         162               84.375  %
Incorrectly Classified Instances        30               15.625  %
Kappa statistic                          0.7613
Mean absolute error                      0.0781
Root mean squared error                  0.2795
Relative absolute error                 23.3639 %
Root relative squared error             68.4377 %
Total Number of Instances              192

=== Detailed Accuracy By Class ===

               TP Rate   FP Rate   Precision   Recall  F-Measure   ROC Area  Class
                 0.75      0.025      0.857     0.75      0.8        0.863    1
                 0.688     0.063      0.688     0.688     0.688      0.813    2
                 0.906     0          1         0.906     0.951      0.953    3
                 0.906     0.167      0.845     0.906     0.874      0.87     4
Weighted Avg.    0.844     0.098      0.846     0.844     0.844      0.873

=== Confusion Matrix ===

  a  b  c  d   <-- classified as
 24  2  0  6 |  a = 1
  1 22  0  9 |  b = 2
  1  1 29  1 |  c = 3
  2  7  0 87 |  d = 4
```

Figure 21. Illustration of SVM classification output result on a testing set.

Now that we have the best parameter set for physical data, could we directly use it to test imaginary dataset? We did another test with all subjects' motor imagery data. As we knew roughly which area the best C and γ would appear, we selected a smaller region to do the loose grid search. We chose C= 2^1, 2^3,… 2^9 and γ=2^{-4}, 2^{-1}, 2^{-3}, …2^{-9}. Figure 22 shows the result, and we can see the best C is around 2^3 and the best γ is around 2^{-3} and the highest classification accuracy is 76.6%.

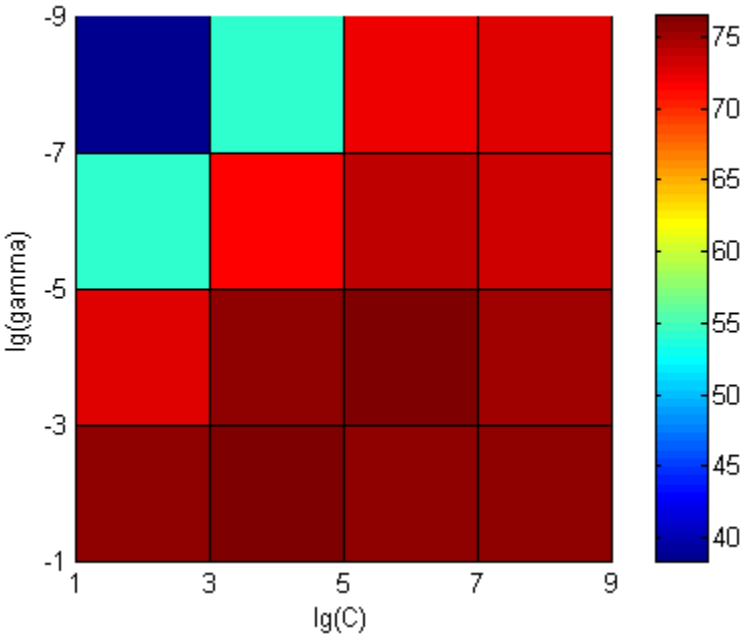

Figure 22. Loose grid search on imaginary data. C= 2^{1}, 2^{3},… 2^{9} and γ=2^{-4}, 2^{-1}, 2^{-3}, …2^{-9}

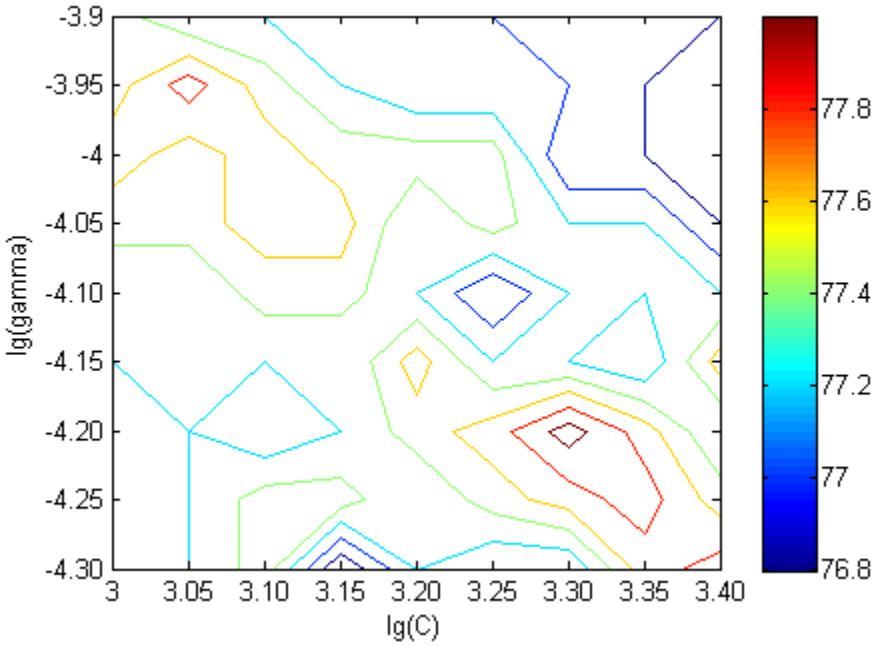

Figure 23. Fine grid search on imaginary data. C= 2^{3}, $2^{3.05}$,… $2^{3.4}$ and γ=$2^{-4.3}$, $2^{-4.25}$, …$2^{-3.9}$

Similarly, fine grid search on the best region was conducted. We chose C= 2^{3}, $2^{3.05}$,… $2^{3.4}$ and γ=$2^{-4.3}$, $2^{-4.25}$, …$2^{-3.9}$. Table 8 shows the fine tuned results using all pairs of C and γ. Figure 23 shows the contour plot of the fine tuned result, and we found that the best pair of C and γ is C= $2^{3.3}$ and γ =$2^{-4.2}$, which made a highest cross validation accuracy of 78.1%. We applied the fine tuned best C and γ to test on each subject's imaginary data, and got the 10-fold cross validation accuracy ranging from 68.2% to 89.6% with the mean of 82.1%. In fact, if we directly applying the best C and γ in physical test to test on each subject's imaginary data, the result ranged from 67.2% to 89.2% with the mean of 82.1% as well, which was very similar to the result using our tuned parameters for imaginary data.

Table 8. Fine tuned cross-validation results using 81 pairs of C and γ

γ \ C	2^{3}	$2^{3.05}$	$2^{3.10}$	$2^{3.15}$	$2^{3.20}$	$2^{3.25}$	$2^{3.30}$	$2^{3.35}$	$2^{3.40}$
$2^{-4.3}$	77	77.2	77.5	76.6	77.2	77	77	77.7	77.9
$2^{-4.25}$	77	77.2	77.5	77.5	77.2	77.5	77.7	77.9	77.5
$2^{-4.20}$	77	77.2	77	77.2	77.5	77.7	78.1	77.7	77.2
$2^{-4.15}$	77.2	77.2	77.2	77.2	77.7	77.2	77.2	77	77.7
$2^{-4.10}$	77.2	77.2	77.5	77.5	77.2	76.8	77.2	77.2	77.2
$2^{-4.05}$	77.5	77.5	77.7	77.7	77.2	77.5	77.2	77.2	76.8
$2^{-4.00}$	77.7	77.5	77.7	77.5	77.5	77.5	76.8	76.8	76.6
$2^{-3.95}$	77.5	77.9	77.5	77.2	77	77	77	76.8	76.6
$2^{-3.90}$	77.5	77.2	77.2	77	77	77	76.8	76.8	76.8

3.3.3 Multilayer perceptron neural network

Compared with logistic regression, the neural network is able to represent more complex models that form non-linear hypotheses. A multilayer perceptron (MLP) is a feedforward artificial neural network model that maps sets of input data onto a set of appropriate output (Figure 24). An MLP consists of multiple layers of nodes, with each layer fully connected to the next one. Except for the input nodes, each node is a neuron (or processing element) with a nonlinear activation function. MLP utilizes a supervised learning technique called backpropagation for training the network. What makes a multilayer perceptron different is that each neuron uses a nonlinear activation function which was developed to model the frequency of action potentials, or firing, of biological neurons in the brain. Learning occurs in the perceptron by changing connection weights after each piece of data is processed, based on the amount of error in the output compared to the expected result. This is carried out through backpropagation.

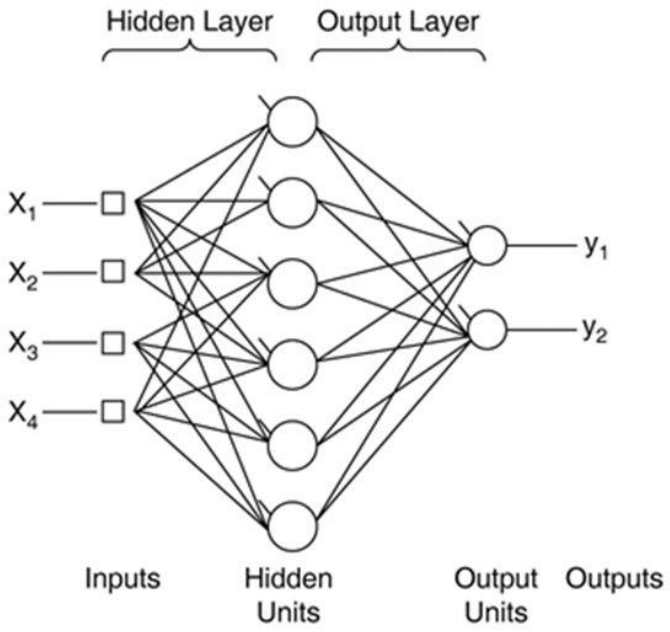

Figure 24. The structure of a multilayer perceptron with one hidden layer of six hidden units.

When training neural networks, it is important to randomly initialize the parameters for symmetry breaking. One effective strategy for random initialization is to randomly select values for $\Theta^{(l)}$ uniformly in the range $[-\epsilon_{init}, \epsilon_{init}]$. We used ϵ_{init} = 0.12. This range of values ensures that the parameters are kept small and makes the learning more efficient.

We set the learning rate $\alpha = 0.3$, so that it wouldn't be too large to diverge the learning. The hidden unit number was initially set to 10, and then we varied this setting to see its affect on the learning algorithm. We tried 5, 10, 15 and 20 (Figure 25) and we found 15 and 20 gave equally good estimates, although no significant difference was observed among all the 4 settings (p-value=0.83). With 15 hidden units, testing accuracy among 5 subjects ranged from 82.5% to 91.3%, with the mean of 87.2%.

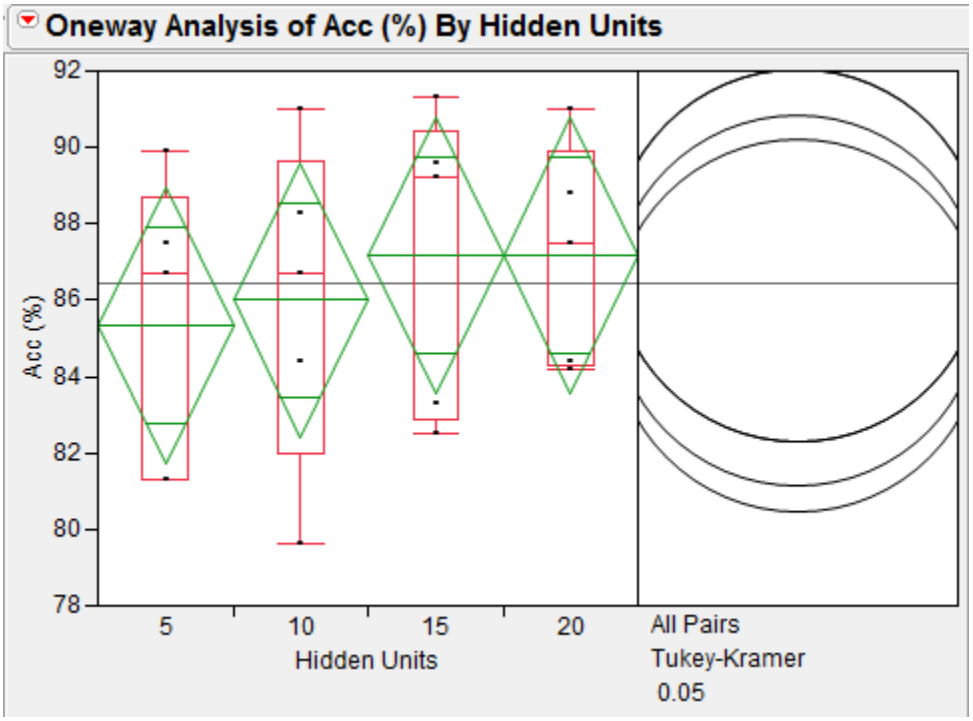

Figure 25. Oneway Anova analysis on different hidden unit effect on the physical data of all subjects.

We then applied MLP on the imaginary data of the 4 subjects who participated, and varied the number of hidden units to see if the same trend could be observed as we saw in physical data. We tried 5, 10, 15 and 20, and we found that (Figure 26) exactly the same trend was observed. With 15 hidden units, classification accuracy ranged from 63.5% to 87.5%, and no significant difference was observed among all the 4 parameter settings (p-value=0.99). This means in the current study, we may just simply apply the best settings in analyzing physical data to analyze imaginary data with a MLP and the result would be as good as using parameters tuned separately on imaginary dataset.

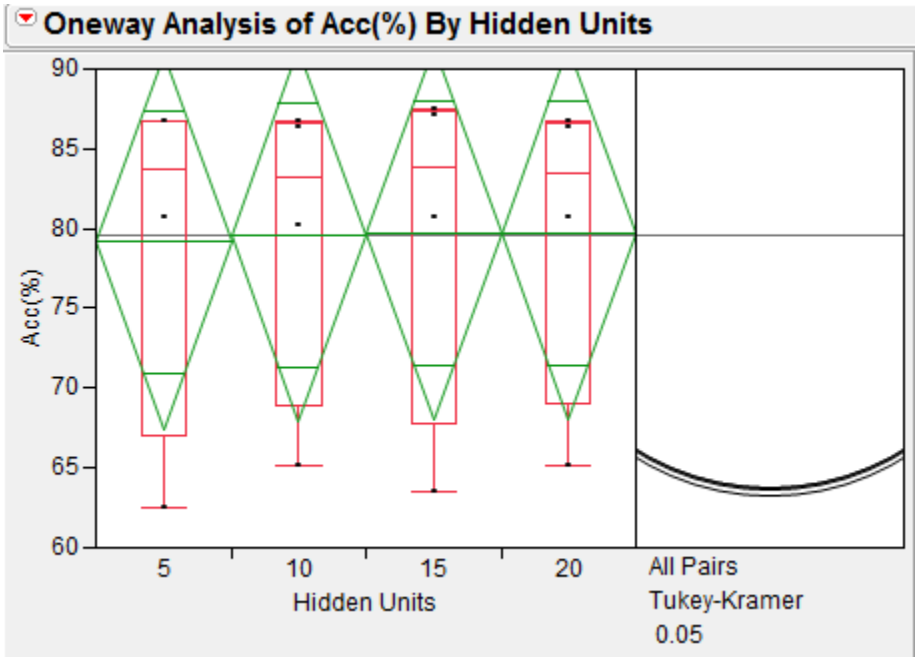

Figure 26. Oneway Anova analysis on different hidden unit effect on the imaginary data of all subjects.

As we have tested the performance for all three classifiers we studied, we would like to make a comparison of their classification accuracy on subjects' physical data. As we can see from Figure 27, MLP gave the highest overall accuracy which was 87.2%; OVA and SVM both had 86.6% accuracy. The performance of three classifiers were not significantly different (p-value=0.96).

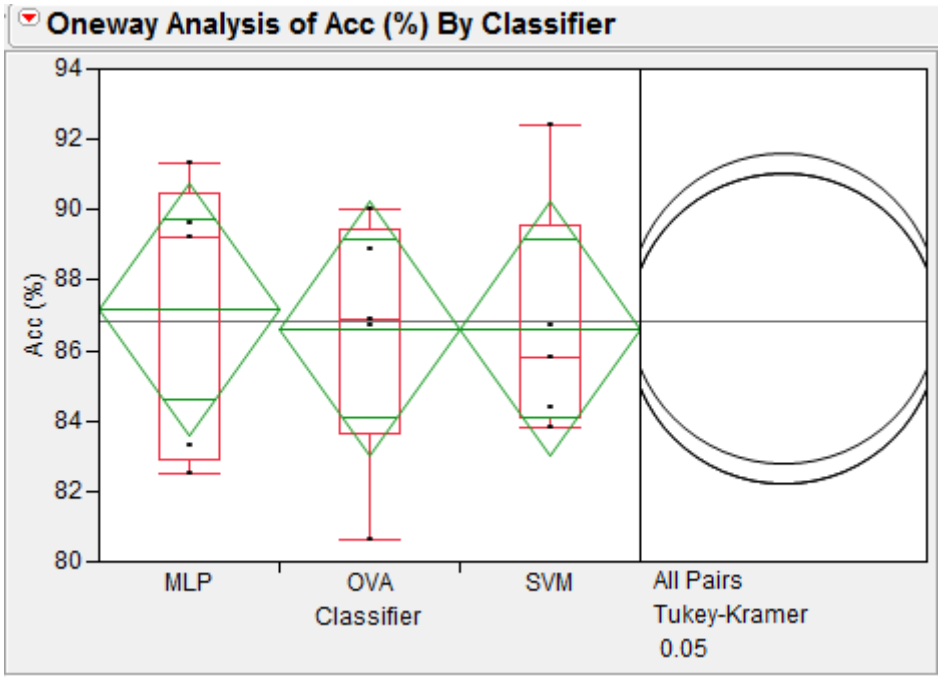

Figure 27. Classifier comparison on physical data.

Table 9 shows the classification results on testing data by all the subjects with all the classifiers, and we statistically compared the performance of classifiers with their optimized settings, and found overall, there was no significant difference among them (p-value=0.95).

Table 9. Comparison of classifiers performance on physical & imaginary data

	Physical			Imaginary		
Accuracy	OVA	SVM	MLP	OVA	SVM	MLP
S1	86.7	86.7	89.2	*	*	*
S2	88.9	92.4	91.3	89.2	83.9	80.7
S3	80.6	83.8	82.5	86.5	89.6	87.1
S4	86.9	85.8	89.6	65	68.2	63.5
S5	90.0	84.4	83.3	77.5	86.7	87.5
Avg	86.6	86.6	87.2	79.6	82.1	79.7
Std	3.63	3.43	4.00	10.99	9.55	11.24

We also compared the performance of physical tasks and imaginary tasks over all the subjects. Figure 28 shows that physical data accuracy was significantly higher than that of imaginary data (p-value=0.03). Physical task classification accuracy was 86.8% with the standard deviation of 1.79%, and imaginary task classification accuracy was 80.5% with the standard deviation of 1.99%. With such accuracy as input signals to the intelligent control system, 95% target hit rate could be obtained for pass-door test and 80% hit rate could be obtained for positioning test under scenes with or without 10 obstacles.

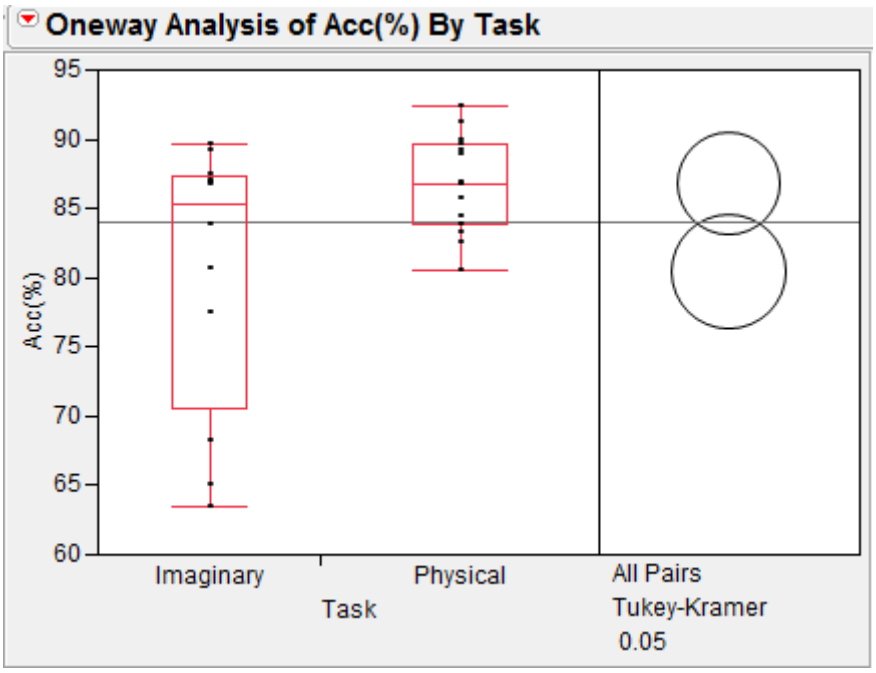

Figure 28. Comparison of physical and imaginary classification accuracies.

3.3.4 Effect of Principle Component Analysis:

When we initially performed test on MLP, we found the classifier training took a long time, even with only 10 hidden units, because we were using 224 features for each dataset. We tried to speed up the learning process by reducing input data dimension, but still wanted to keep adequate variance to best present the data, so we performed Principle Component Analysis (PCA). Often, its operation can be thought of as revealing the internal structure of the data in a way which best explains the variance in the data. If a multivariate dataset is visualized as a set of coordinates in a high dimensional data space, PCA can supply the user with a lower-dimensional picture, a "shadow" of this object when viewed from its most informative viewpoint. This is done by using only the first few principal components so that the dimensionality of the transformed data is reduced.

We chose to keep 95% variance of the data, and tested on each individual's physical dataset. The testing accuracy was obviously lower (75.4% to 85.1%) compared to the results of OVA or SVM, but the learning speed was greatly enhanced, as feature numbers were reduced to 52 to 60 for 5 subjects, compared with previously used 224. By reducing feature numbers, we may have lost useful information for classification, so we kept the original 224 features, and performed MLP tests again on each subject.

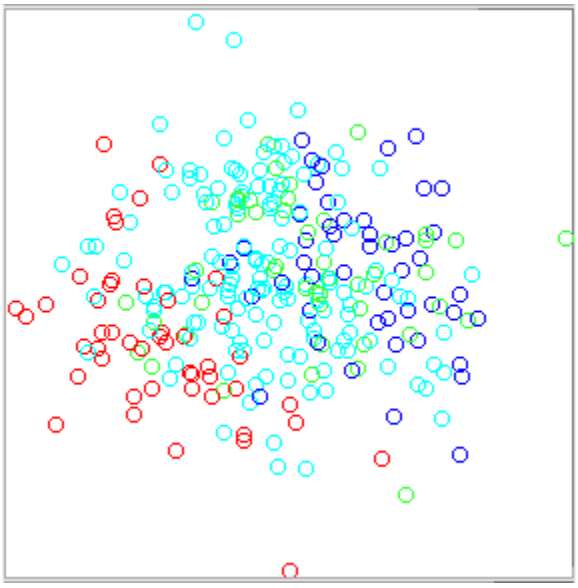

Figure 29. Instances projection onto the plane of 2 PCA selected features: good separation of class 1 (blue) and 2 (red)

It is of interest to take a closer look at the data distributions on different feature plane. Figure 29 is an illustration of input data distribution of subject 2's physical data. The data were projected onto a plane defined by two features. In this picture, blue circles represent

GS tasks or right hand continuous movements, red circles are LT tasks or left hand short movement, green circles are RT tasks or right hand short movement and light blue ones are ID tasks or idle state data. We can see that red and blue circles are easier to be separated compared to being separated from others, which means the two features played an important role in separating this two tasks, but may not be very helpful for separations of other pairs by only using this two features. While in Figure 30, red, blue and green tasks may be quite separable by another two features alone.

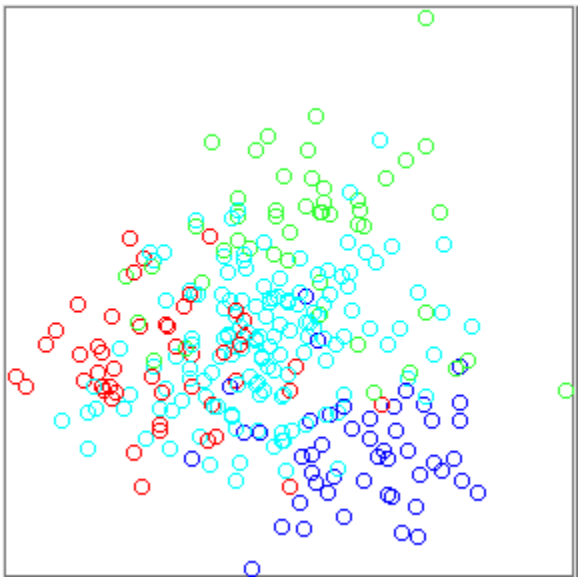

Figure 30. Instances projection onto another plane of 2 PCA selected features: good separation of red, blue and green classes.

Figure 31 shows an example of data presented by PCA selected features. Each sub picture is a data projection on to a plane formed by a pair of the selected features.

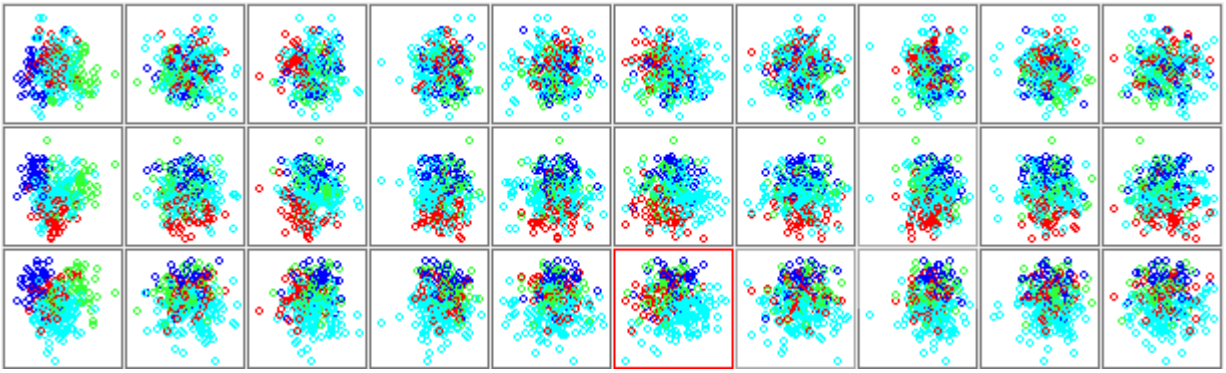

Figure 31. Visualization of a subset features of PCA selected features.

3.3.5 Recommendation on classifier selection

Beyong the exploration that we have shown above, we also did a lot of preliminary test on varying different parameters of classifiers, different number of features, and different size of training and testing data. Altough the classifier performance seen from the current results shows no much difference among the 3 classifiers, we still have a general recommendation that should be applicable to similar problems.

Out of the 3 methods we have used, logistical regression, support vector machines and neural network, we define m to be the training sample size, and n to be the number of features, then

- If n is large (relative to m), for example, $n \geq m, n = 10000, m = 10 \ldots\ldots 1000$, logistic regression or SVM with a linear kernel should be considered.
- If n is small, m is intermediate, for example, $n = 1 \ldots\ldots 1000, m = 10 \ldots\ldots 10000$, then SVM with Gaussian kernel is good to use, which is the case in our study.

- If n is small, m is large, for example, $n = 1 \ldots \ldots 1000, m = 50000$, then more features need to be added or created, and logistic regression or SVM without a kernel should be used.
- Neural network is likely to work well for most of these settings, but may be slower to train compared with some learning algorithms.

CHAPTER 4

SSVEP for Hybrid BCI system

4.1 Background and significance

Although years of research in improving EEG signal quality has contributed a lot to the accuracy and speed of decoding human intentions, it is reported that around 20% of subjects do not exhibit the performance for effective BCI control. It becomes a top priority when designing a BCI. Recently, hybrid BCI systems have been increasingly adopted in many applications [12-15], as they combine good features of different BCI systems and show advantages than traditional BCIs. The idea of hybrid BCI has been carried out in binary cursor control, and preliminary test reported enhanced universality [14, 15]. The central hypothesis is that a hybrid BCI for the proposed 2D control by combining steady-state visual evoked potential (SSVEP) and event-related desynchronization/ synchronization (ERD/ERS) based BCI systems would exhibit comparable control accuracy but enhanced universality than single BCI system in this case. The ultimate goal of this study is hoping to enhance the universality of/let more people use our BCI system by combining two BCI systems, i.e. (1) imagined hand movement with SMR based BCI, and (2) visual attention task with steady-state visual evoked potential (SSVEP) BCI. The resulting hybrid BCI would have both tasks simultaneously. In the current study, we focused on designing and testing the SSVEP system as the SMR-based ERD/ERS system has been built in the previous studies. We would in the future combine the two systems so

that a hybrid BCI could be implemented into a wheelchair control system which would be of high accuracy, decent speed and good universality.

Previous studies in 2D non-invasive cursor control/wheelchair control were mostly sensorimotor rhythm (SMR)-based. Although reports for real-time control strongly implicated the potential of SMR-based BCI system, control accuracies were far from optimal. Some adopted P300 in target selection when controlling a wheelchair in a situation that the map is known, and the navigation was done by control system. However, in the real world, map is usually unknown, and BCI users have to go through the process control. SSVEP has recently been used in binary or 2D controls as it has distinguishable features and high detection speed. In the binary control, SSVEP was used as a part of a hybrid BCI system. It combined with ERD-based BCI system which showed improved universality, and therefore, we hope that combined SSVEP and ERD/ERS BCI may also exhibit improved usability in 2D control. We first wanted to test how the SSVEP alone performs in 2D control. In a 2D control study which SSVEP was used, four programmed flashing squares were surrounding a virtual car on its four sides, providing stimuli. Detection of staring at each flashing light corresponded to the car moving to one direction. In this case, subjects had to stare at one flashing light as the classifier could only distinguish among the four frequency responses of staring at the four stimuli. We believe that the paradigm could be improved to be more user-friendly so that subjects don't need to stare at the flashing stimulus when they don't want to control the car. We proposed that the classification of not looking at the light source could be more difficult when applying the

methods used for traditional SSVEP paradigm, and approaches such as power spectrum analysis may be helpful to distinguish it from other responses of looking at stimuli.

4.2 Experimental design of SSVEP paradigm

We use three flashing LEDs of different frequencies to provide visual stimuli as control signals.

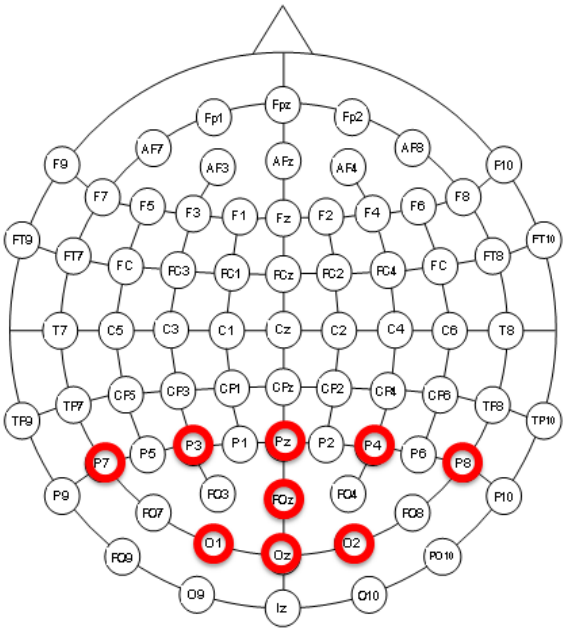

Figure 32. Electrodes used (in red circles) in SSVEP study.

Data collection:

Figure 32 shows the electrodes setup in this study. Nine channels (P7, P3, Pz, P4, P8, POZ, O1, OZ, and O2) according to the International 10-20 system of electrode placement were

selected for EEG recording in the SSVEP-based BCI system, as they lie in the strong activated areas near the occipital and parietal lobes. A ground electrode was placed on site AFZ on the forehead, and all channels were referenced to the right ear lobe. All impedances were kept below 5k. Data were band-pass filtered between 0.5 and 100 Hz, amplified, and sampled at 256 Hz. Data were collected and analyzed using Matlab BCI2VR toolbox.

System setup and experimental paradigm:

Figure 33A shows the LED driving circuit, which was consisted of three NE555 sub-circuits. Frequencies designed for the LED flashing rates are 7.62Hz, 10.27Hz and 12.7Hz. By choosing RC circuit parameters, we considered the flashing duty cycle as well and set it to 0.4, under which studies have shown that visual response is highest. Figure 33B and C show how the LEDs are fixed on the screen: sitting in front of the computer, LED flashing at 7.62Hz is on the central left side of the screen, on the central top is the 10.27Hz one, and on the right side is the 12.7Hz LED. Fig. 11C shows the paradigm. Three LEDs were flashing at from the beginning of the experiment through the end. In each trial, one of the four cues (“left”, “up”, “right” and “down”) shows up in the center of the screen for 1s, indicating that subject should focus on the LED on that direction. When a beep onset, subject started to stare at the LED for 4s until the beep offsets and subject shifts attention back to the center, waiting for the next trial. When the cue indicated “down”, subject slightly looked down, focus on the lower area on the screen, as there is no LED, subject did not receive any particular 16 visual stimuli. There were thirty trials in each direction,

with 1s break between every two trials and 5s break after every 10 trials. All together, 120 trials took 13 minutes.

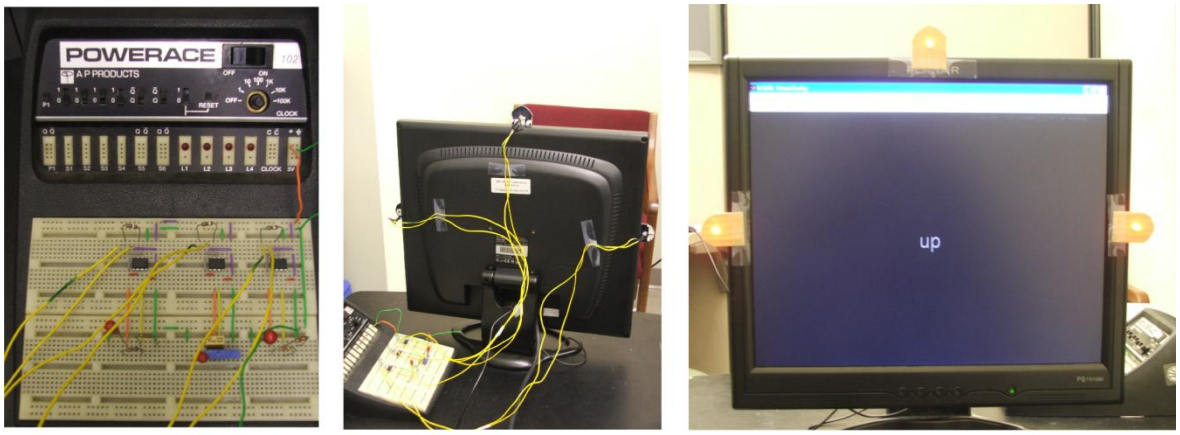

Figure 33. System setup and experimental paradigm. A. LED driving circuit, output frequencies of square waves are 7.62Hz, 10.27Hz and 12.7Hz, with duty cycle 0.4. B. Experimental setup. C. Positions of the three LEDs and the experimental paradigm.

4.3 Data analysis:

To determine proper classification methods, we first examined the SSVEP responses to three LED stimuli and one non-stimulus. We observed that the visual responses to three flashing LEDs exhibit clear peaks at corresponding fundamental frequencies and show unclear pattern when subjects do not stare at any LEDs. Figure 34 gives an example of the data from one subject who participated in this study. Periodogram of channel 9 in each trial was calculated and plotted, and then 19 trials of PSD for each task were averaged to get one subplot in Figure 34, with the frequency resolution 0.125Hz.

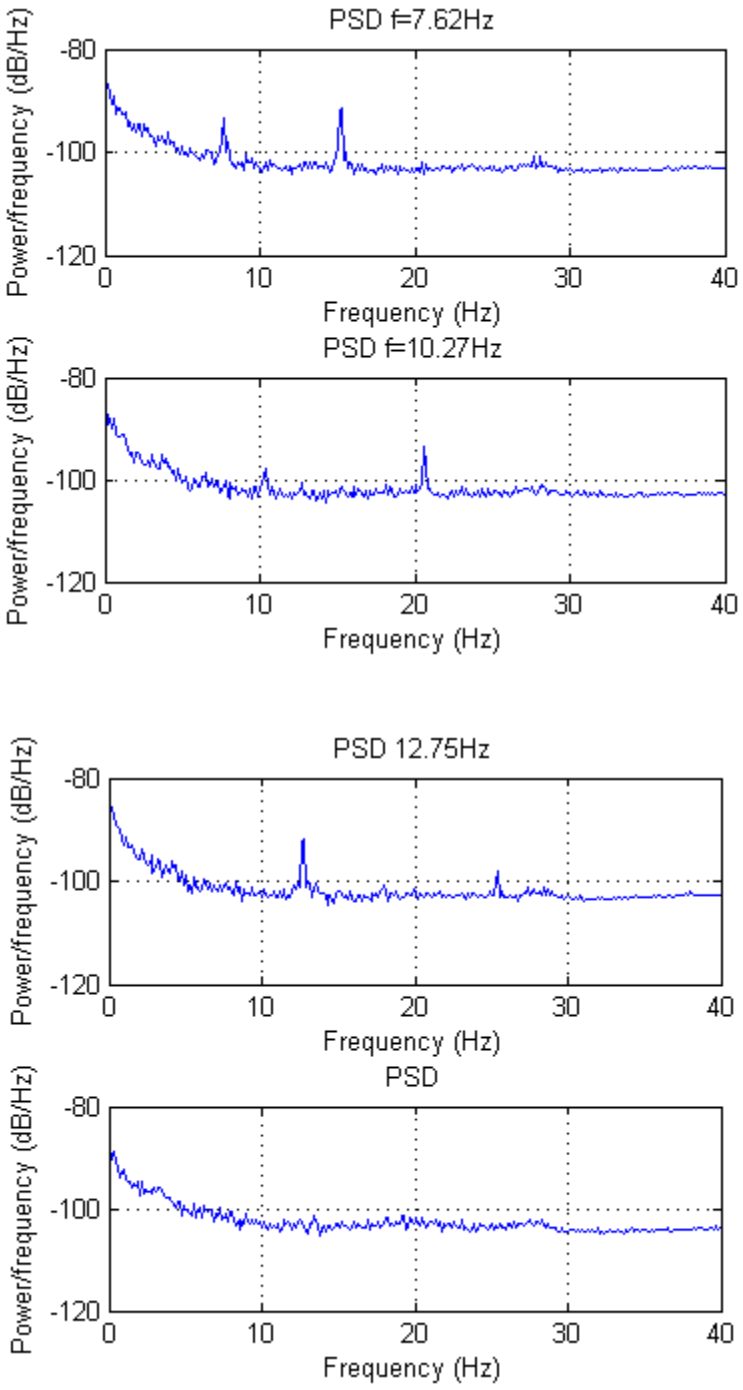

Figure 34. Averaged power spectrum density of visual responses. From top to down: PSD of stimulus with f=7.62Hz; PSD of stimulus with f=10.27Hz; PSD of stimulus with f=12.75Hz and PSD of not staring at any stimulus.

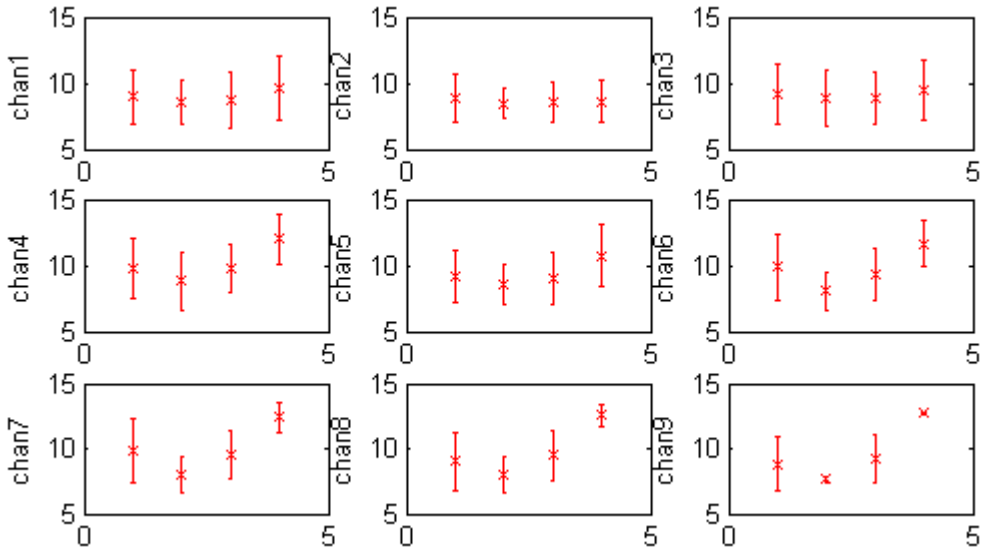

Figure 35. Distribution of peak values for class 1-4 ("down", "left", "up", and "right") of each channel 1-9.

From Figure 34 we can see that fundamental frequencies can be visually observed as well as their second harmonics in the averaged PSD. Except for the trials without staring at stimulus, by looking at where the largest peak occurs (from 7Hz to 13Hz), we can distinguish those three stimuli frequencies. Classification method by Voting (9 channels) gave an 88% classification accuracy. Figure 35 shows the distribution of peak values for class 1-4 (corresponding to "down", "left", "up" and "right" cases) of channels 1 to 9. From the distribution we can see that channel 1-5 does not provide good separability of the four classes, even the best channel 9 cannot guarantee good performance in the testing as the standard deviations of "down" and "up" are relatively high. In some trials, components of second harmonics can be more obvious than the fundamental frequency peaks. Thus, a

method which can recognize the frequency with a harmonic relationship can greatly improve the performance of the BCI.

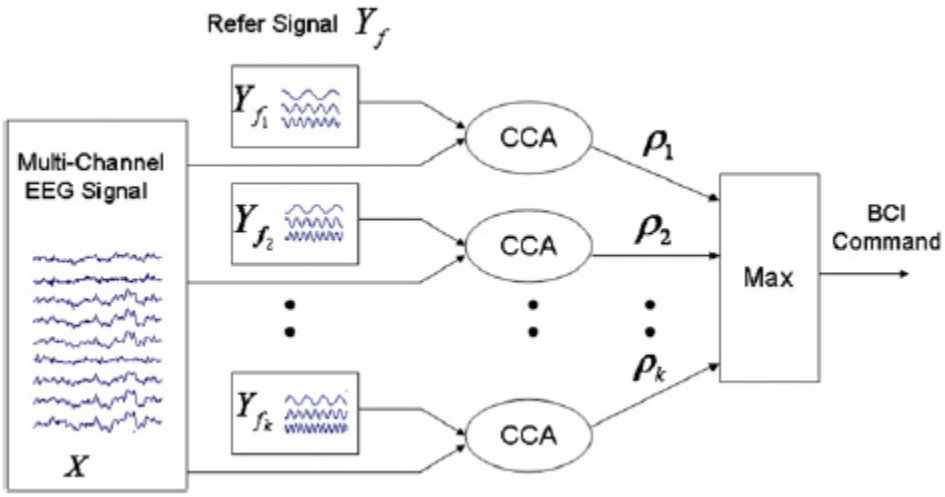

Figure 36. An illustration for usage of CCA in EEG signals analysis. X is the 9 channel EEG signals. Yf1-Yf3 are the reference signals with f1-f3 Hz stimulus frequencies.

Recently, the use of a canonical correlation analysis (CCA) method for multi-channel SSVEP detection has showed highly increased detection accuracy. CCA is a multivariable statistical method used when there are two sets of data which may have underlying correlation. CCA finds a pair of linear combinations, for two sets, such that the correlation between the two canonical variables is maximized. As explained in Figure 36, the input multi-channel EEG signals were the 9 channels SSVEP signals we had. We created reference signal Y_f. Y_f was set as:

$$Y_f = \begin{pmatrix} \sin(2\pi f t) \\ \cos(2\pi f t) \\ \bullet \\ \bullet \\ \sin(2\pi N_h f t) \\ \cos(2\pi N_h f t) \end{pmatrix},$$

Where N_h was the number of harmonics. The 9 channel EEG signals and each of the reference signals was used as an input of the CCA method. The output canonical correlation ρ could be used for frequency recognition. The user's command C was recognized as C=maxρ, i=1,2,..., k, Where ρ_i were the CCA coefficients obtained with the frequency of reference signals being f_1, f_2,…, f_k.

We tested CCA on one subject's dataset. When we used information of 4s length of data, 3 harmonics, and all 9 electrodes, the classification accuracy got 95% for the three classes with stimulation. To distinguish Idle from classes with stimulations, we used PSD method. We chose 4Hz frequency bin; 4 features were selected by GA from 9 SSVEP channels and 2-9 frequency bins, and MLD classifier provided 90% classification accuracy.

CHAPTER 5

Summary and future work

5.1 Contributions and future work

5.1.1 Practical design of 2D wheelchair control

This study presented a novel and effective virtual wheelchair control system design, which incorporated a non-control state with state control strategy. It applied the rationale of our previous 2D cursor control, yet further redesigned and extended it. The wheelchair could be operated to turn left or right, to go straight or stop, with all the basic motion functions that a real wheelchair has. The prominent induced power decrease (ERD) and power increase (ERS) associated with imagined natural movements allowed the reliable discrimination of movement intentions, and therefore improved control accuracy and increased the degrees of freedom of the wheelchair control system. One major improvement of the implemented virtual wheelchair is its ability to move continuously, instead of the previous step by step control of a 2D cursor.

The control process is very user friendly. It is in a manner similar to driving, when people want to start the engine, finish turning and go straight, or stop during emergency, they step firmly on the accelerator or brake for a period. Drivers hold this state when they don't want to change direction or stop, which is similar to the non-control state in this study where subject remained relaxed, and doesn't have to control their brain rhythms every single

moment which was done in conventional rhythm control wheelchair systems just to keep the wheelchair on the right track. This gave subjects 2-4.5s intervals between two active commands which allowed them to take a break and get prepared for the next movement. For the condition that they kept moving/ turning, the non-control state allowed even longer relaxation time for the subjects, or for the potential paralyzed patients. The current design aimed at ease of use for the potential user while keeping a reliable sense of control, with good control speed.

We expect that subjects would improve their control skills quickly in the potential later studies, considering that subjects achieved comparable performances as S2 who had several hours of previous BCI experience. Compared to the current EEG-based continuous 2-D BCIs that require months of subject training and may cause fatigue in the long run, the proposed BCI system exhibited prominent advantages. In brief, the results proved the feasibility of the ERD/ERS based brain-controlled virtual wheelchair system, which subjects could rapidly attain a significant level of control with a short calibration period. In the future research, we would consider how to develop asynchronous wheelchair control based on the current system to further increase control speed while maintaining reasonable control accuracy. The implementation of this virtual wheelchair control provided a valuable system prototype for the research in the field of rehabilitation wheelchair. Both control signals and control mechanism can be expanded flexibly to implement more complex and intelligent control systems.

5.1.2 Exploration of pattern recognition methods

In this study, three important classifiers, i.e., One-vs-All logistic regression classifier, Support vector machine classifier and Multilayer perceptron classifier were carefully studied, and their parameters were tuned in order to achieve good predictions on the new data. We discussed in details why we chose those parameters to change, and performed tests on training and testing datasets on both individuals' and pooled data to learn the effects. We also plotted learning curve to evaluate whether over-fitting or under-fitting existed in the learning process, how the error was of the classifier and discuss possible further improvements such as reduce feature numbers or enlarge dataset size when possible. Meanwhile, we also pointed out and conducted comparisons on several issues that deserved attention when applying these classifiers to the data, such as scaling data on different features before applying classification algorithms, and randomly initializing weight parameters for MLP to avoid network symmetry.

Our optimized classifiers gave comparable results with each other, and classification accuracies were all above 80% for 5 subjects' physical data. According to our simulation output of human-wheelchair cooperation with integrated intelligent control, using the output signals of the classifiers as the input signals of the simulated system, pass-door tasks and positioning tasks would obtain an average hit rate of above 95% and 80% respectively, even with up to 10 obstacles in the scenes. The optimization results provided the human-wheelchair system with further information and feedback, which can be used to

further guide the improvement of system and algorithm design and simulation.

Considering the integrity of this research work, we briefly conclude our collaboration work with the robotics team. In the simulation study, a human-wheelchair cooperative approach to of reliable planning and execution was tested. The system consists of three components: human user, wheelchair and the noninvasive BCI which can represent limit types of user's intention patterns based on EEG signals, with varying decoding accuracy and time delay. To achieve efficient navigation and positioning, three cooperative modes were proposed for specific situations depending on the trade-off of wheelchair's autonomy and user's flexibility. The respective coding protocol and error-tolerance strategy of each mode were studied, and strategies of mode switching among three cooperative modes were developed. To achieve continuous and smooth motion, the wheelchair predicted next intermediate path segment based on the historic decisions from visual feedback, so that the user could adjust the intention and actively correct extraction error of the BCI, and finally determine the wheelchair's next action, before the wheelchair reached the current path node. Combining such predictive control strategy with cooperative modes, reliable planning and execution were ensured, even under the conditions of low decoding accuracies of the BCI. The effectiveness of the strategies was evaluated by simulations. This study further extended the application scenarios of the EEG based wheelchair control, as it incorporated automatic obstacle avoidance and navigation, reliable path planning and fault-tolerant strategy, and dealt with control under insufficient accuracy of input decoded EEG signals. It provided system response feedback to the EEG signal decoding part and paved the way for a real

wheelchair system.

5.1.3 SSVEP system for the hybrid BCI

The 2D SSVEP system design and implementation have been tested in the EEG experiments, and were approved of high performance without much complex algorithms or high demand of mental load. Further test in the larger population whether people generally perform well with the current SSVEP based 2D BCI and what percentage of people who cannot benefit from SSVEP BCI can perform well on SMR based BCI will be of interest to conduct.

Using a second BCI approach might help conveying user's intent if the first one cannot sufficiently do so, as more useful features in the second approach can be included to decode user intention together with the original features in the first BCI system. Especially the hybrid BCIs could improve information throughput if users exhibit both types of features. 2D BCI control system is the basic component of our research system, and the wheelchair control system is an extension of its application. The SSVEP-BCI system in this study serves as an assistive component aiming to increase the possibility of usage among people.

Literature Cited

1. Pope AM, T.A., *Disability in America: Toward a national agenda for prevention.* Washington (DC): National Academy Press, 1991.
2. Iezzoni LI, M.E., Davis RB, Siebens H., *Mobility difficulties are not only a problem of old age.* J Gen Intern Med., 2001. **16**(4): p. 235-43.
3. Hayashi, H. and E.A. Oppenheimer, *ALS patients on TPPV: totally locked-in state, neurologic findings and ethical implications.* Neurology, 2003. **61**(1): p. 135-7.
4. Hanssens, Y., et al., *Improving oral medicine administration in patients with swallowing problems and feeding tubes.* Ann Pharmacother, 2006. **40**(12): p. 2142-7.
5. Bromberg, M.B., *Quality of life in amyotrophic lateral sclerosis.* Phys Med Rehabil Clin N Am, 2008. **19**(3): p. 591-605, x-xi.
6. Williams, L.M., et al., *General and social cognition in first episode schizophrenia: identification of separable factors and prediction of functional outcome using the IntegNeuro test battery.* Schizophr Res, 2008. **99**(1-3): p. 182-91.
7. Lule, D., et al., *Life can be worth living in locked-in syndrome.* Prog Brain Res, 2009. **177**: p. 339-51.
8. Mutsaarts, M., B. Steenbergen, and R. Meulenbroek, *A detailed analysis of the planning and execution of prehension movements by three adolescents with spastic hemiparesis due to cerebral palsy.* Exp Brain Res, 2004. **156**(3): p. 293-304.

9. Daly, J.J., et al., *A randomized controlled trial of functional neuromuscular stimulation in chronic stroke subjects.* Stroke, 2006. **37**(1): p. 172-8.

10. Ring, H. and N. Rosenthal, *Controlled study of neuroprosthetic functional electrical stimulation in sub-acute post-stroke rehabilitation.* J Rehabil Med, 2005. **37**(1): p. 32-6.

11. Alon, G., et al., *A home-based, self-administered stimulation program to improve selected hand functions of chronic stroke.* NeuroRehabilitation, 2003. **18**(3): p. 215-25.

12. Wolf, S.L., et al., *Effect of constraint-induced movement therapy on upper extremity function 3 to 9 months after stroke: the EXCITE randomized clinical trial.* JAMA, 2006. **296**(17): p. 2095-104.

13. Joseph, A.B., *Design considerations for the brain-machine interface.* Med Hypotheses, 1985. **17**(3): p. 191-5.

14. Kennedy, P.R., et al., *Direct control of a computer from the human central nervous system.* IEEE Trans Rehabil Eng, 2000. **8**(2): p. 198-202.

15. Wolpaw, J.R., et al., *Brain-computer interfaces for communication and control.* Clin Neurophysiol, 2002. **113**(6): p. 767-91.

16. Daly, J.J. and J.R. Wolpaw, *Brain-computer interfaces in neurological rehabilitation.* Lancet Neurol, 2008. **7**(11): p. 1032-43.

17. Birbaumer, N. and L.G. Cohen, *Brain-computer interfaces: communication and restoration of movement in paralysis.* J Physiol, 2007. **579**(Pt 3): p. 621-36.

18. Sitaram, R., et al., *Temporal classification of multichannel near-infrared spectroscopy signals of motor imagery for developing a brain-computer interface.* Neuroimage, 2007. **34**(4): p. 1416-27.

19. Velliste, M., et al., *Cortical control of a prosthetic arm for self-feeding.* Nature, 2008. **453**(7198): p. 1098-101.

20. Birbaumer, N., et al., *The thought translation device (TTD) for completely paralyzed patients.* IEEE Trans Rehabil Eng, 2000. **8**(2): p. 190-3.

21. Wolpaw, J.R. and D.J. McFarland, *Multichannel EEG-based brain-computer communication.* Electroencephalogr Clin Neurophysiol, 1994. **90**(6): p. 444-9.

22. Wolpaw, J.R. and D.J. McFarland, *Control of a two-dimensional movement signal by a noninvasive brain-computer interface in humans.* Proc Natl Acad Sci U S A, 2004. **101**(51): p. 17849-54.

23. Iversen, I., et al., *Conditional associative learning examined in a paralyzed patient with amyotrophic lateral sclerosis using brain-computer interface technology.* Behav Brain Funct, 2008. **4**: p. 53.

24. Sykacek, P., et al., *Probabilistic methods in BCI research.* IEEE Trans Neural Syst Rehabil Eng, 2003. **11**(2): p. 192-5.

25. Birbaumer, N., *Breaking the silence: brain-computer interfaces (BCI) for communication and motor control.* Psychophysiology, 2006. **43**(6): p. 517-32.

26. Kubler, A., et al., *The thought translation device: a neurophysiological approach to communication in total motor paralysis.* Exp Brain Res, 1999. **124**(2): p. 223-32.

27. Kubler, A., et al., *Brain-computer communication: self-regulation of slow cortical potentials for verbal communication.* Arch Phys Med Rehabil, 2001. **82**(11): p. 1533-9.

28. Hill, N.J., et al., *Classifying EEG and ECoG signals without subject training for fast BCI implementation: comparison of nonparalyzed and completely paralyzed subjects.* IEEE Trans Neural Syst Rehabil Eng, 2006. **14**(2): p. 183-6.

29. Birch, G.E., Z. Bozorgzadeh, and S.G. Mason, *Initial on-line evaluations of the LF-ASD brain-computer interface with able-bodied and spinal-cord subjects using imagined voluntary motor potentials.* IEEE Trans Neural Syst Rehabil Eng, 2002. **10**(4): p. 219-24.

30. Blankertz, B., et al., *The non-invasive Berlin Brain-Computer Interface: fast acquisition of effective performance in untrained subjects.* Neuroimage, 2007. **37**(2): p. 539-50.

31. Sellers, E.W. and E. Donchin, *A P300-based brain-computer interface: initial tests by ALS patients.* Clin Neurophysiol, 2006. **117**(3): p. 538-48.

32. Wolpaw, J.R., et al., *An EEG-based brain-computer interface for cursor control.* Electroencephalogr Clin Neurophysiol, 1991. **78**(3): p. 252-9.

33. Birbaumer, N., et al., *A spelling device for the paralysed.* Nature, 1999. **398**(6725): p. 297-8.

34. Nijboer, F., et al., *A P300-based brain-computer interface for people with amyotrophic lateral sclerosis.* Clin Neurophysiol, 2008. **119**(8): p. 1909-16.

35. Karim, A.A., et al., *Neural internet: Web surfing with brain potentials for the completely paralyzed.* Neurorehabil Neural Repair, 2006. **20**(4): p. 508-15.

36. Tanaka, K.M., K. ; Wang, H.O. , *Electroencephalogram-based control of an electric wheelchair*. IEEE Trans Robotics, 2005. **21**(4): p. 762 - 766

37. Rebsamen, B.B., E. ; Guan, C. ; Haihong Zhang ; Chee Leong Teo ; Qiang Zeng ; Ang, M. ; Laugier, C. , *A brain-controlled wheelchair based on P300 and path guidance*. Biomedical Robotics and Biomechatronics, 2006: p. 1101 - 1106

38. Galan, F., et al., *A brain-actuated wheelchair: asynchronous and non-invasive Brain-computer interfaces for continuous control of robots.* Clin Neurophysiol, 2008. **119**(9): p. 2159-69.

39. Pfurtscheller, G. and F.H. Lopes da Silva, *Event-related EEG/MEG synchronization and desynchronization: basic principles.* Clin Neurophysiol, 1999. **110**(11): p. 1842-57.

40. Leeb, R. and G. Pfurtscheller, *Walking through a virtual city by thought.* Conf Proc IEEE Eng Med Biol Soc, 2004. **6**: p. 4503-6.

41. Del, R.M.J.J., et al., *Asynchronous non-invasive brain-actuated control of an intelligent wheelchair.* Conf Proc IEEE Eng Med Biol Soc, 2009. **2009**: p. 3361-4.

42. McFarland, D.J. and J.R. Wolpaw, *EEG-based communication and control: speed-accuracy relationships.* Appl Psychophysiol Biofeedback, 2003. **28**(3): p. 217-31.

43. Krusienski, D.J., et al., *A mu-rhythm matched filter for continuous control of a brain-computer interface*. IEEE Trans Biomed Eng, 2007. **54**(2): p. 273-80.

44. Royer, A.S. and B. He, *Goal selection versus process control in a brain-computer interface based on sensorimotor rhythms.* J Neural Eng, 2009. **6**(1): p. 016005.

45. Royer, A.S., et al., *EEG control of a virtual helicopter in 3-dimensional space using intelligent control strategies.* IEEE Trans Neural Syst Rehabil Eng, 2010. **18**(6): p. 581-9.

46. Vanacker, G., et al., *Context-based filtering for assisted brain-actuated wheelchair driving.* Comput Intell Neurosci, 2007: p. 25130.

47. Bell, C.J., et al., *Control of a humanoid robot by a noninvasive brain-computer interface in humans.* J Neural Eng, 2008. **5**(2): p. 214-20.

48. Kim, H.K., et al., *Continuous shared control for stabilizing reaching and grasping with brain-machine interfaces.* IEEE Trans Biomed Eng, 2006. **53**(6): p. 1164-73.

49. McFarland, D.J., W.A. Sarnacki, and J.R. Wolpaw, *Electroencephalographic (EEG) control of three-dimensional movement.* J Neural Eng, 2010. **7**(3): p. 036007.

50. Pfurtscheller, G., *Functional topography during sensorimotor activation studied with event-related desynchronization mapping.* J Clin Neurophysiol, 1989. **6**(1): p. 75-84.

51. Magnani, G., et al., *Event-related desynchronization to contingent negative variation and self-paced movement paradigms in Parkinson's disease.* Mov Disord, 1998. **13**(4): p. 653-60.

52. Szurhaj, W., et al., *Event-related variations in the activity of EEG-rhythms. Application to the physiology and the pathology of movements.* Epileptic Disord, 2001. **Special Issue**: p. 59-66.

53. Bai, O., et al., *A high performance sensorimotor beta rhythm-based brain-computer interface associated with human natural motor behavior.* J Neural Eng, 2008. **5**(1): p. 24-35.

54. Kayagil, T.A., et al., *A binary method for simple and accurate two-dimensional cursor control from EEG with minimal subject training.* J Neuroeng Rehabil, 2009. **6**: p. 14.

55. Salmelin, R., et al., *Functional segregation of movement-related rhythmic activity in the human brain.* Neuroimage, 1995. **2**(4): p. 237-43.

56. Neuper, C. and G. Pfurtscheller, *Evidence for distinct beta resonance frequencies in human EEG related to specific sensorimotor cortical areas.* Clin Neurophysiol, 2001. **112**(11): p. 2084-97.

57. Cassim, F., et al., *Does post-movement beta synchronization reflect an idling motor cortex?* Neuroreport, 2001. **12**(17): p. 3859-63.

58. Pfurtscheller, G., *Event-related synchronization (ERS): an electrophysiological correlate of cortical areas at rest.* Electroencephalogr Clin Neurophysiol, 1992. **83**(1): p. 62-9.

59. Pfurtscheller, G., A. Stancak, Jr., and C. Neuper, *Event-related synchronization (ERS) in the alpha band--an electrophysiological correlate of cortical idling: a review.* Int J Psychophysiol, 1996. **24**(1-2): p. 39-46.

60. Pfurtscheller, G., et al., *Beta rebound after different types of motor imagery in man.* Neurosci Lett, 2005. **378**(3): p. 156-9.

61. Huang, D., et al., *Decoding human motor activity from EEG single trials for a discrete two-dimensional cursor control.* J Neural Eng, 2009. **6**(4): p. 046005.

62. Bai, O., et al., *Towards a user-friendly brain-computer interface: initial tests in ALS and PLS patients.* Clin Neurophysiol. **121**(8): p. 1293-303.

63. Jasper, H.H. and H.L. Andrews, *Electro-encephalography. III. Normal differentiation of occipital and precentral regions in man.* Arch Neurol Psychiat, 1938. **39**: p. 95-115.

64. Bai, O., et al., *Exploration of computational methods for classification of movement intention during human voluntary movement from single trial EEG.* Clin Neurophysiol, 2007. **118**(12): p. 2637-55.

65. Simpson, R., et al., *The smart wheelchair component system.* J Rehabil Res Dev, 2004. **41**(3B): p. 429-42.

66. Babiloni, F., et al., *Multimodal integration of high-resolution EEG and functional magnetic resonance imaging data: a simulation study.* Neuroimage, 2003. **19**(1): p. 1-15.

67. Hjorth, B., *An on-line transformation of EEG scalp potentials into orthogonal source derivations.* Electroencephalogr Clin Neurophysiol, 1975. **39**(5): p. 526-30.

68. Nunez, P.L., et al., *EEG coherency. I: Statistics, reference electrode, volume conduction, Laplacians, cortical imaging, and interpretation at multiple scales.* Electroencephalogr Clin Neurophysiol, 1997. **103**(5): p. 499-515.

69. Welch, P.D., *The Use of Fast Fourier Transform for the Estimation of Power Spectra:A Method Based on Time Averaging Over Short, Modified Periodograms* IEEE Trans. Audio Electroacoust 1967. **AU-15**: p. 70-73

70. Mitra, P.P. and B. Pesaran, *Analysis of dynamic brain imaging data.* Biophys J, 1999. **76**(2): p. 691-708.

71. Percival, D.B.a.A.T.W., *Spectral Analysis for Physical Applications: Multitaper and Conventional Univariate Techniques* Cambridge: Cambridge University Press. , 1993.

72. Huan, N.J. and R. Palaniappan, *Neural network classification of autoregressive features from electroencephalogram signals for brain-computer interface design.* J Neural Eng, 2004. **1**(3): p. 142-50.

73. Raymer, M.L., et al., , *Dimensionality reduction using genetic algorithms* IEEE Transactions 2000. **4**(2): p. 164-71.

74. Marques, J.P., *Pattern recognition: concepts, methods and applications* Berlin: Springer-Verlag 2001.

75. Chatterjee, A., et al., *A brain-computer interface with vibrotactile biofeedback for haptic information.* J Neuroeng Rehabil, 2007. **4**: p. 40.

76. Fawcett, T., *ROC graphs: notes and practical considerations for data mining researchers.* 2003.

77. Leeb, R., et al., *Brain-computer communication: motivation, aim, and impact of exploring a virtual apartment.* IEEE Trans Neural Syst Rehabil Eng, 2007. **15**(4): p. 473-82.

78. McFarland, D.J., et al., *Brain-computer interface (BCI) operation: signal and noise during early training sessions.* Clin Neurophysiol, 2005. **116**(1): p. 56-62.

VITA

Dandan Huang was born in November 1984, in Tianjin, China. She got her B.S. degree in the School of Precision Instrument and Opto-Electronics Engineering in 2007 with a major of Biomedical Engineering at Tianjin University in China. She worked as a research assistant in the Bio-Instrumentation and Imaging Lab at Virginia Commonwealth University (VCU), and obtained her M.S. degree in 2009. She continued with her Ph.D. study in Biomedical Engineering, EEG&BCI Lab, VCU, where she is currently a research assistant. Her research interests include Signal processing & Machine learning, Brain-computer interface, Rehabilitation robotics and Medical devices.

Dandan was invited to be a member in Phi Kappa Phi Honor Society and AEMB Biomedical Engineering Honor Society. She is also a member in the IEEE Society, IEEE Engineering in Medicine and Biology Society, IEEE Women Engineers Society, and IEEE Communications Society.

She has published 15 first-authored and co-authored book chapters, journal/conference papers/abstracts, which have been quickly cited for 40 times. Since 2010, she has been invited to review 30 manuscripts for 8 leading journals, such as IEEE Transactions on Neural System and Rehabilitation Engineering, Clinical Neurophysiology, Journal of Neural Engineering, and Journal of NeuroEngineering and Rehabilitation.